Geochemistry and petrography of amphibolites from the Spuhler Peak Metamorphic Suite near the Branham Lakes area, Tobacco Root Mountains, southwestern Montana

An Honors Thesis submitted to the faculty of
Washington and Lee University as partial fulfillment
of the requirements for the degree of
Bachelor of Science in Geology

by

Michael Jason Cox

Department of Geology
Washington and Lee University
Lexington, Virginia 24450
May 1996

All our knowledge brings us nearer to our ignorance.

-"The Rock"; T. S. Eliot, 1934

TABLE OF CONTENTS

ABSTRACT

Located in the west-central Tobacco Root Mountains in southwestern Montana, the Archean-aged Spuhler Peak Metamorphic Suite (SPMS) of Gillmeister (1972) consists of lensoid amphibolite beds, more equant bodies of "wispy" amphibolite, pods of ultramafic rock, hornblende-plagioclase gneisses, garnet-gedrite gneisses, quartzites, and sillimanite schists structurally overlying the Indian Creek Metamorphic Suite (ICMS) to the south and west and resting beneath the Pony-Middle Mountain Metamorphic Suite (PMMMS) to the north (Burger, 1969). The concern of this report, SPMS amphibolites from a variety of locations mostly within the area from Noble Peak and Mustard Pass in the northwest to Lower Branham Lake in the southeast have been analyzed for their major and trace element chemistry. As determined by Niggli trends and a variety of diagnostic geochemical criteria, the SPMS amphibolites are concluded to have been derived from an igneous and not sedimentary protolith. Tectonic discriminant diagrams based on elements generally considered immobile during metamorphism predominately indicate correspondence to modern-day ocean floor basalts (OFB), though some ambiguity exists. The plots of the SPMS amphibolites on the tectonic discrimination diagrams are somewhat dispersed as well, possibly due to composition changes caused by the relatively high grade of metamorphism that affected the amphibolites. This dispersion combined with a lack of detailed information regarding plate-tectonics in the Archean complicates the accuracy of interpreting the basalt-type for the SPMS amphibolites.

INTRODUCTION

Amphibolites pose a problem to geologists attempting to constrain a protolith as they may form from the metamorphism of a basalt or gabbro, basalt tuff or tuff mixed with carbonate, calcareous shale or shaley limestone, the metasomatic replacement of marble, or the replacement of pyroxene granulite (metasediment) **(Table 1)** (Hyndman, 1985). The existence of amphibolite layers within metasedimentary sequences further creates difficulties in determining origins, especially when the rocks are so deformed that any original intrusive or sedimentary relationships have been eradicated. Such is the case with the amphibolites, both the lenses and the more equant bodies, concordantly interlayered within the metasedimentary schists, gneisses, and quartzites of the Spuhler Peak Metamorphic Suite (SPMS) of the Tobacco Root Mountains in southwestern Montana. Field observations of these amphibolites provide little evidence concerning their origin. While some outcrops possess a planar foliation and a mineral lineation, these characteristics do not necessarily indicate a sedimentary protolith for metamorphic rocks (Leake, 1969). This study concentrates on

identifying the protolith of this sequence of rocks through an evaluation of its petrography and, in more detail, geochemistry. Deducing the protolith and tectonic setting of the SPMS amphibolites can provide a better understanding of Archean crustal development in this region.

GEOLOGIC SETTING

One of the north westernmost ranges in the Wyoming Crustal Province (Condie, 1969) of the North American shield, the glaciated high peaks of the Tobacco Root Mountains represent an uplifted range cored with Archean supracrustal sequences that have been intruded by the Cretaceous Tobacco Root Batholith during the Laramide orogeny **(Fig. 1)**. Flanked by Paleozoic and Mesozoic sedimentary sequences that drape its northern and western sides, the interior of the Tobacco Root Range consists of three main suites of Archean metamorphic rock that sit in contact with each other and the granite batholith that was emplaced 73 million-years ago. Located in the west-central part of the range, the Spuhler Peak Metamorphic Suite (SPMS) **(Fig. 2)** resembles a northwest- trending sliver that hugs the western side of the batholith. Composed of lensoid amphibolite layers, more equant, "wispy" amphibolite, hornblende-plagioclase gneisses, pods of ultramafic rock, garnet-gedrite gneisses, quartzites, and sillimanite schists, the SPMS overlies the predominately metasedimentary Indian Creek Metamorphic Suite (ICMS) to the south and west and underlies the Pony-Middle Mountain Metamorphic Suite (PMMMS) to the north (Burger, 1969). The contact between the SPMS and the other units, interpreted to be a fault with related zones of local shearing (Burger, 1969) and an unconformity surface (Gillmeister, 1972), is not well understood. Based on geochemistry, Cummings and McCulloch (1989) believe that the SPMS represents a slice of oceanic crust that has been thrust on top of shelf sediments. Perhaps further investigation of the petrography and geochemistry of the SPMS amphibolites will provide more

insight into how the various SPMS lithologies relate to each other and their structural neighbors.

PETROGRAPHY

While most thin sections demonstrate characteristics common to amphibolites, variations in mineral composition and texture do occur. The samples vary in color, mineral content, and grain size. Few thin sections show any preferred orientation. Most of the samples consist of the assemblage hornblende-plagioclase-quartz, with varying amounts (if any) of garnet, biotite, chlorite, cummingtonite, ground-up material termed "grunge", and opaques such as magnetite and pyrite. The color of the hornblende ranges from green to brown. Samples collected adjacent to the contact with the late Mesozoic Tobacco Root Batholith contain more biotite probably due to alteration by contact with this hot body. Muscovite and biotite are more abundant in samples from the Leggat cirque area near the contact with the ICMS than in most of the other SPMS amphibolites. Garnet increases in abundance in the disturbed zone (up to 45%) and as one approaches the contact with the ICMS, suggesting higher pressure. The anorthite content of the plagioclases in different samples ranges from Ab70-An30 to Ab35-An65, with an average of Ab60-An40. The varying modal amounts of hornblende and plagioclase, sometimes with significant amounts of quartz, suggests that some samples are hornblende-plagioclase-quartz gneisses. **Table 2** provides a brief summary of the petrography of the SPMS amphibolites.

GEOCHEMISTRY

Thirty-one of the more than two-hundred SPMS amphibolite samples collected in the field were selected for chemical analyses of major and trace elements by XRF at XRAL Laboratories or at Franklin and Marshall College in Lancaster,

Pennsylvania. Major elements were determined on glass discs fused with lithium tetraborate, and trace elements on pressed powder pellets. Rare earth element analysis data were obtained for the same 31 samples by instrumental neutron activation analysis at the University of Virginia. The results of these analyses are presented in **Tables 3 and 4**. This geochemical data was then used to determine a protolith and tectonic setting for the SPMS amphibolites as a whole.

Nature of parent rocks: ortho- vs. para-amphibolites

The problem of distinguishing between ortho- and para-amphibolites has troubled many geologists, but few new methods have been developed in the last 25 years to accomplish it. Nevertheless, it is generally agreed that chemical trends serve as the best mechanism of discriminating between igneous and sedimentary protoliths for amphibolites (Leake, 1964). In several studies, Leake (1964, 1969) arrives at a solution for constraining fields for igneous versus sedimentary protoliths for amphibolites by means of variation diagrams using Niggli values (1954). van de Camp (1969) likewise used Niggli values to determine the origin of amphibolites from the nearby Beartooth Mountains, Montana, finding them to show igneous trends. **Table 5** shows the Niggli values calculated for the SPMS amphibolites.

The SPMS amphibolite samples used in this report plot in an area where a trend from anorthosite toward basalts crosses an area of clay and dolomite mixtures on a plot of al-alk vs. *c* **(Fig. 3)** (Leake, 1969). This diagram fails to support unequivocally either a sedimentary or igneous origin for the protolith. A plot of *c* versus *mg* **(Fig. 4)** is a more conclusive diagram as it indicates that the SPMS amphibolites follow the same trend as the Karroo dolerites (Evans and Leake, 1960). In addition, the SPMS samples follow the trend from early basic to late basic igneous rocks when plotted on a 100*mg+c+(al-alk) diagram **(Fig. 5)** (Leake, 1963).

Considering the significant changes in bulk chemical composition that can ensue during high grade metamorphism event, it is crucial to examine trends using trace elements, especially for elements that demonstrate relative immobility. In plots of *mg* vs. Cr **(Fig. 6)** and *mg* vs. Ni **(Fig. 7)** (Evans and Leake, 1960), the SPMS amphibolites have trends with positive slopes such as those found in igneous but not shale-carbonate rocks. It is not possible for para-amphibolite rocks such as mixtures of pelite and carbonate to produce the range in Ni and Cr values shown by the SPMS amphibolites. Para-amphibolites would produce a negative correlation, while these amphibolites, like ortho-amphibolites, demonstrate a positive correlation between *mg* and Cr and *mg* and Ni (Sills and Tarney, 1984). Thus the protolith of the SPMS amphibolites must be igneous.

Nature of Igneous Protolith:

The SPMS amphibolite data were plotted on the Alkali-Silica diagram to characterize the basalt protolith. Such a plot **(Fig. 8)** shows the SPMS amphibolites plotting in the subalkaline field. The SPMS amphibolites plot as picro-basalts, basalts, basalt andesites, and andesites on the total alkali-silica diagram **(Fig. 9)** (LeBas et al., 1986). On a P2O5 vs. Zr diagram **(Fig. 10)**, the SPMS amphibolites plot as tholeiitic and not alkaline. All of the SPMS samples also plot in the field of tholeiitic and not calc-alkaline on an AFM diagram **(Fig. 11)**. However, 3 samples (#12, #32, and #36B) plot as calc-alkaline while the rest plot as tholeiitic basalts on a FeO/MgO vs. SiO2 diagram **(Fig. 12)** (Miyashiro, 1974). Thus most of the SPMS amphibolites can be interpreted as derived from tholeiitic basalts.

Tectonic Classification and Significance:

A number of workers have used variation diagrams to correlate various compositional parameters with modern tectonic environments (Pearce and Cann, 1973, Pearce and Norry, 1979, Mullen, 1983, and Meschede, 1986). Pearce and Cann

utilized discriminant analysis to assign basalts to modern tectonic settings of eruption, identifying ocean floor basalts (OFB) with diverging plate margins, volcanic arc basalts (VAB) with converging plate margins, ocean island basalts (OIB) with within-plate oceanic crust, and continental basalts (CB) with within plate-continental crust. Plots of SPMS amphibolites on some of these tectonic discrimination diagrams do not correlate their protoliths with a single tectonic environment. Pearce and Cann (1973) express reservations in regard to using tectonic discrimination diagrams for rocks produced during Archaen volcanic events since so little is known about the rate of magma production and the nature of plate tectonics before the Cambrian period.

Many geologists use the elements Ti, Zr, and Y for discriminating tectonic environments because of their relative obstinateness to secondary processes. Cann (1970) shows that these elements can be utilized to identify ocean-floor basalts when positive correlations exist between Zr and Ti and Y and Ti. In the case of the SPMS amphibolites, positive slopes occur when these plots are produced **(Figs. 13 & 14)**, suggesting that these samples may have an ocean-floor parent basalt. Similarly, a modified plot of Zr vs. Ti **(Fig. 15)** (Pearce and Cann, 1973) shows SPMS amphibolites lying in the fields of ocean-floor basalts (12), island-arc basalts (6), calc-alkali basalts (4), and in a field containing OFB, IAB, and CAB (6). A plot of Zr-(Ti/100)-(Y*3) **(Fig. 16)** (Pearce and Cann, 1973) shows a distribution in the fields of OFB (19 samples), calc-alkali basalts (CAB) (5), and within-plate basalts (OIB or CB) (4).

Using other immobile trace elements, a plot of Zr-Ti/100-Sr/2 **(Fig. 17)** (Pearce and Cann, 1973) shows the SPMS amphibolites plotting in the fields of OFB (13), IAB (5), and CAB (7). Y/Nb ratios **(Table 6)** used in determining petrologic character (Pearce and Cann, 1973) also suggest that the majority of the SPMS amphibolites originally formed as ocean-floor basalts as 26 samples have a ratio greater than 3. On

a plot of Ti vs. Cr **(Fig. 18)** (Pearce and Cann, 1973), 20 of the 31 SPMS samples plot almost evenly in the fields of low-K tholeiites associated with an island-arc origin (11) and ocean-floor basalts (9). A Zr/Y-Zr plot **(Fig. 19)** (Pearce and Norry, 1979) shows the SPMS samples plotting in the fields of island-arc basalts (7), ocean-ridge basalts (12), within-plate basalts (4), and some (8) outside these boundaries.

A K2O-TiO2-P2O5 diagram (Pearce et al., 1975), used to discriminate between oceanic and non-oceanic basalts, indicates that most of the SPMS amphibolites originated in an oceanic environment **(Fig. 20)**. This plot does not represent a viable tectonic discriminator though as some continental basalts such as the Scoresby Sund and Deccan Traps Tertiary basalts plot in the oceanic field (Pearce et al., 1975). The SPMS amphibolites appear to be more constrained in a Pearce plot using the major elements MgO-FeO(total)-Al2O3 **(Fig. 21)** (Pearce et al., 1977). In it they appear largely confined to the ocean-island basalt field (20), with a few (6) plotting in the continental basalt field and (3) in the ocean ridge field.

A Nb-Zr-Y plot **(Fig. 22)** (Meschede, 1986) indicates that the SPMS amphibolites are distributed between four tectonic environments: normal-MORB/volcanic-arc basalts (15), plume-type-MORB/VAB (7), within-plate tholeiites (1), and OFB/LKT/CAB (4). Volcanic-arc basalts and MORB's are not clearly distinguishable on this diagram. On a plot of MnO-TiO2-P2O5 **(Fig. 23)** (Mullen, 1983), the SPMS amphibolites plot in the fields of island-arc tholeiites (16), CAB (13), and MORB (1).

Most of the tectonic discrimination diagrams, especially those of Pearce and Cann (1973), suggest that the SPMS amphibolites have an ocean-floor basalt as a protolith. A summary of the distributions of SPMS amphibolites to tectonic environments is shown in **Tables 7 and 8.**

Spider Diagrams:

Multi-trace element plots can be used for some lithologies including amphibolites to demonstrate an affinity with the chemical signature of parent rocks

such as back-arc basin basalts, island-arc tholeiites, and calc-alkaline basalts (Chalokwu and Hanley, 1990). In this study, sampling was conducted for the trace elements Ba, Cr, Cu, Ga, Nb, Ni, Rb, Sr, Th, Ti, U, V, Y, Zn, and Zr in the SPMS amphibolites. Composition values for the individual 31 samples and the mean, mean + standard deviation, and mean - standard deviation values calculated from the SPMS amphibolites are presented for interpretation and comparison ease on spider diagrams **(Figs. 24 and 25)**. These spider plots for normal-type MORB-normalized incompatible elements in the SPMS amphibolites show only the trace elements Ba, Nb, Rb, Sr, Th, Ti, U, and Y.

The compositional patterns shown by the SPMS amphibolites in these spider diagrams **(Figs. 24 and 25)** (Sun and McDonough, 1989) demonstrate only a close similarity to the pattern for a back-arc basin basalt when compared to the basalt-types plotted by Weaver et al. (1979), Saunders and Tarney (1979), and Wilson (1989) in **figures 26 and 27**. More specifically, patterns for the SPMS amphibolite samples **(Figs. 24 and 25)** resemble patterns given by a back-arc basin (BAB) basalt from the Bransfield Strait and Scotia Sea **(Fig. 26)** (Weaver et al., 1979, and Saunders and Tarney, 1979). Rb and Ba in some of the SPMS samples are much more enriched than in the BAB basalts. Patterns of depletion in Nb, a chemical signature characteristic of all arc basalts, and enrichment of K in the SPMS amphibolites and the BAB basalts show similarities. Mid-ocean ridge basalts and island arc tholeiites do not show a Nb depletion **(Fig. 27)**. La, Ce, and Sr compositions for the amphibolites and their possible protolith appear to match. One of the samples (#24D) does demonstrate a considerable depletion in Sr though, contrary to patterns given by the BAB basalts. While not shown for the BAB basalts, Nd compositions for the SPMS amphibolites differ considerably as 9 samples are enriched and 6 samples are depleted. The patterns of depletion in Zr, Ti, and Y for the amphibolites and BAB basalts exhibit a similar behavior.

Rare-Earth-Element Analysis:

Rare-earth elements constitute a special class of trace elements that can prove useful in trying to understand the formation and evolution of magmas (Hyndman, 1985). Assuming closed-system conditions, the REE content of a metamorphic rock such as amphibolite may imitate the REE content of the parent rock (Grauch, 1989). In this study, the SPMS amphibolites were sampled for the light REEs: La, Ce, Nd, and Sm, and the heavy REEs: Gd, Yb, and Lu, and all were normalized to chondritic meteorites. While all the 31 samples were plotted in **figure 28**, plots of the mean, mean + standard deviation, and mean - standard deviation values for each of the REE were graphed for viewing simplification **(Fig. 29)**.

With varying degree, the REE concentrations of the SPMS amphibolites show the same general pattern on a chondrite-normalized plot **(Figs. 28 and 29)** (Nakamura, 1974). Relative to chondrites, all of the samples are enriched in light REE and heavy REE. With respect to each other though, the SPMS amphibolite samples demonstrate a pattern of enrichment in light REE and a slight depletion in HREE. Gd shows an unexpected and anomolous depletion in all the samples. For further ease of comparison with standard REE values devised from other workers, **figure 30** shows the average REE + or - one standard deviation without the unusually high depletion in Gd. This extreme depletion in Gd is not seen in the REE patterns for other amphibolites such as those of Sills and Tarney (1984). These amphibolites instead demonstrate Gd enrichment **(Fig. 31)**.

The average LREE values range from *8 to *50 chondrite-normalized and average HREE values extend from *3 to *15 chondrite-normalized on **figure 29**. In the graph showing REE patterns for all 31 individual samples **(Fig. 28)**, values for LREE range from *5 to *100 chondrite-normalized and HREE values range from *2 to *25 chondrite-normalized. Several of the samples, namely samples #6, #21B, #29D, #32,

#33D, and #39C, exhibit depletions in Nd. Sample #33D further shows an unusual depletion in Ce.

The overall REE pattern of the SPMS amphibolites does not resemble the REE patterns described for basalts from mid-ocean ridges, island-arcs, or the Andes plotted by Hyndman **(Fig. 32)**, or arc tholeiites, rise tholeiites, Hawaiian tholeiites, Hawaiian alkali basalts, or oceanic-island alkali basalts plotted by Condie **(Fig. 33)**. Furthermore, LREE and HREE patterns for the SPMS amphibolites seem to fit in the zone for many types of basalts and granite **(Fig. 32)**. Considering that they do not closely correlate with any one pattern common to the many types of parent basalts, one can conclude that the SPMS amphibolites have experienced one or more episodes of high-grade metamorphism that has altered the chemical signature of their protolith. Though the question of REE mobility has been debated for years, the problem has not been resolved (Grauch, 1989). The failure of the REE pattern for the SPMS amphibolites to correspond to any of the examples cited in the literature suggests that these REE behaved in a mobile fashion.

CONCLUSIONS

The geochemistry of the SPMS amphibolites assigns certain constraints in terms of understanding the source of their protoliths as well as deducing a tectonic environment in which these protoliths first formed. From the plots originally devised by Evans and Leake (1960), the SPMS amphibolites are interpreted to be of igneous and not sedimentary origin. Other plots **(Figs. 8, 9, 10, 11, & 12)** characterize the igneous protolith of the SPMS amphibolites as subalkaline and tholeiitic basalts. While plots on tectonic discrimination diagrams are somewhat dispersed possibly due to composition changes caused by the relatively high grade of metamorphism, most samples plot as ocean floor basalts (OFB) associated with a spreading center. Spider plots of normal-type mid-oceanic ridge basalts (n-MORB) normalized

incompatible elements in the SPMS amphibolites demonstrate that the SPMS amphibolites possess a chemical signature pattern that closely coincides with that of back-arc basin basalts (BAB). Like MORBs, back-arc basin basalts are associated with a rift environment (Misra and Conte, 1991). Some workers believe that it is impossible to discriminate between ocean floor basalts generated at a mid-ocean ridge or at a back-arc basin (Misra and Conte, 1991). One should note, however, that back-arc basin basalts show a characteristic Nb depletion while MORB's and ocean island tholeiites demonstrate a Nb enrichment **(Fig. 27)**. Since all of the SPMS amphibolites exhibit a depletion in Nb, one can deduce that the amphibolites' parent basalt formed in a back arc basin tectonic environment. Thus, the protolith of the SPMS amphibolites most probably is an ocean floor basalt that formed at a diverging plate margin (Pearce and Cann, 1973), namely in a back-arc basin **(Figs. 34 & 35)**. One should remain cautious though in making interpretations about tectonic environments as a lack of detailed information regarding plate-tectonics in the Archean still exists.

ACKNOWLEDGMENTS

I am grateful to Dr. H. Robert Burger, Dr. Jack Cheney, Dr. John Brady, and Dr. Tekla Harms for introducing me to the geology of such a grand study area, and Dr. Bernard E. Leake, whose timely correspondence via email allowed me to solve many problems. Thanks to my field partner Kathy Degraaf of Amherst College, whose observations in the field helped me out tremendously. I wish to thank the Washington and Lee Department of Geology, including Dr. Ed Spencer, Dr. Fred Schwab, Dr. David Harbor, Bob Thren, Sue Woodruff, and Deborah Hubbard, for their valuable time in assisting me with the technical and administrative sides of performing this project. I would like to acknowledge the W. M. Keck Foundation, the Keck Consortium, and Washington and Lee University for financial support at various stages of the project. I wish to extend my appreciation to Franklin and Marshall College for use of their analytical facilities, and the University of Virginia's Reaction Facility for providing REE analysis. Finally, I must express my appreciation to my thesis advisor, Dr. Sam Kozak, for his advice and contributions to this report. Thank you all very much.

REFERENCES CITED

Burger, H. R., 1969, Structural evolution of the southwestern Tobacco Root Mountains, Montana: Geological Society of American Bulletin, v. 80, p.1329-1342.

Cann, J. R., 1970, Rb, Sr, Y, Zr and Nb in some ocean floor basaltic rocks: Earth and Planetary Science Letters, v. 10, p. 7-11.

Chalokwu, C. I., and Hanley, T. B., 1990, Geochemistry, petrogenesis, and tectonic setting of amphibolites from the southernmost exposure of the Appalachian Piedmont: Journal of Geology, v. 98, p. 725-738.

Condie, K. C., 1976, Plate Tectonics and Crustal Evolution: New York, Pergamon Press, 310 p. [book]

Cordua, W. S., 1973, Precambrian Geology of the Southern Tobacco Root Mountains, Madison County, Montana [Ph.D. thesis]: Indiana University, Bloomington, Indiana, 248 p.

Cummings, M. L., and McCulloch, W. R., 1988, Geochemistry and origin of amphibolite and ultramafic rocks, Branham Lakes area, Tobacco Root Mountains, southwestern Montana *in* Bartholomew, M. J., Hyndman, D. W., Mogk, D. W., and Mason, R., eds., Basement Tectonics 8: Characterization and comparison of ancient and Mesozoic continental margins- Proceedings of the 8th International Conference on Basement Tectonics (Butte, Montana, 1988): Dordrecht, The Netherlands, Kluwser Academic Publishers, p. 323-340.

Evans, B. W., and Leake, B. E., 1960, The Composition and Origin of the Striped Amphibolites of Connemara, Ireland: Journal of Petrology, v. 1, p. 337-363.

Gillmeister, N. M., 1972, Cherry Creek Group-Pony Group relationship in the central Tobacco Root Mountains, Madison County, Montana: Northwest Geology, v. 1, p. 21-24.

Grauch, R. I., 1989, Rare Earth Elements in metamorphic rocks *in* Lipin, B. R., and McKay, G. A., eds., Geochemistry and Mineralogy of Rare Earth Elements: Reviews in Mineralogy, v. 21, p. 147-167.

Hyndman, D. W., 1985, Petrology of Igneous and Metamorphic Rocks: New York, McGraw-Hill, 786 p. [book]

Leake, B. E., 1963, Origin of amphibolites from Northwest Adirondacks, New York: Geological Society of America Bulletin, v. 74, p. 1193-1202.

Leake, B. E., 1964, The Chemical Distinction Between Ortho- and Para-amphibolites: Journal of Petrology, v. 5, p. 238-254.

Leake, B. E., 1969, The Discrimination of Ortho and Para Charnokitic Rocks, Anorthosites and Amphibolites: The Indian Mineralogist, v. 10, p. 89-104.

LeBas, M. J., LeMaitre, R. W., Streckeisen, A., and Zanettin, B., 1986, A chemical classification of volcanic rocks based on the total alkali silica diagram: Journal of Petrology, v. 27, p. 745-750.

Meschede, M., 1986, A Method of Discriminating Between Different Types of Mid-Ocean Ridge Basalts and Continental Tholeiites with the Nb-Zr-Y Diagram: Chemical Geology, v. 56, p. 207-218.

Misra, K. C., and Conte, J. A., 1991, Amphibolites of the Ashe and Alligator Back Formations, North Carolina: Samples of Late Proterozoic-early Paleozoic oceanic crust: Geological Society of America Bulletin, v. 103, p. 737-750.

Miyashiro, A., 1974, Volcanic rock series in island arcs and active continental margins: American Journal of Science, v. 274, p. 321-355.

Mullen, E. D., 1983, MnO/TiO2/P2O5: a minor element discrimination for basaltic rocks of oceanic environments and its implications for petrogenesis: Earth and Planetary Science Letters, v. 62, p. 53-62.

Nakamura, N., 1974, Determination of REE, Ba, Fe, Mg, Na and K in carbonaceous and ordinary chondrites: Geochemica et Cosmochimica Acta, v. 38, p. 757-775.

Niggli, P., 1954, Rocks and Mineral Deposits: San Francisco, W. H. Freeman and Company, 559 p. [book]

Pearce, J. A.., and Cann, J. R., 1973, Tectonic Setting of Basic Volcanic Rocks Determined Using Trace Element Analyses: Earth and Planetary Science Letters, v. 19, p. 290-300.

Pearce, J. A., and Norry, M. J., 1979, Petrogenetic implications of Ti, Zr, Y, and Nb variations in volcanic rocks: Contributions to Mineralogy and Petrology, v. 69, p. 33-47.

Pearce, T. H., Gorman, B. E., and Birkett, T. C., 1975, The TiO2-K2O-P2O5 Diagram: A method of discriminating between oceanic and non-oceanic basalts: Earth and Planetary Science Letters, v. 24, 419-426.

Pearce, T. H., Gorman, B. E., and Birkett, T. C., 1977, The relationship between major element chemistry and tectonic environment of basic and intermediate volcanic rock: Earth and Planetary Science Letters, v. 36, p. 121-132.

Saunders, A. D., and Tarney, J., 1979, The geochemistry of basalts from a back-arc spreading center in the East Scotia Sea: Geochemica et Cosmochimica Acta, v. 43, p. 555-572.

Sills, J. D., and Tarney, J., 1984, Petrogenesis and tectonic significance of amphibolites interlayered with metasedimentary gneisses in the Ivrea Zone, Southern Alps, Northwest Italy: Tectonophysics, v. 107, p. 187-206.

Sun, S.-s, and McDonough, W. F., 1989, Chemical and isotopic systematics of oceanic basalts: implications for mantle compositions and processes *in* Saunders, A. D., and Norry, M. J., Magmatism in the Oceanic Basins: Geol. Soc. Spec. Pub. No. 42, p. 313-345.

van de Camp, P. C., 1969, Origin of Amphibolites in the Beartooth Mountains, Wyoming and Montana: New Data and Interpretation: Geological Society of America Bulletin, v. 80, p. 1127-1136.

Weaver, S. D., Saunders, A. D., Pankhurst, R. J., and Tarney, J., 1979, A geochemical study of magmatism associated with the initial stages of back-arc spreading: Contributions to Mineralogy and Petrology, v. 68, p. 151-169.

Windley, Brian F., 1984, The Evolving Continents: Chichester, John Wiley & Sons, 399 p. [book]

Wilson, Majorie, 1989, Igneous Petrogenesis: A Global Tectonic Approach: London, Unwin Hyman, 466 p. [book]

APPENDIX A: TABLES

Table 1: Suggested protoliths for amphibolites (Hyndman, 1985).

Possible origin	Criteria used for determination
Metamorphism of basalt or gabbro sill, dike, or pluton	Commonly homogeneous and unlayered, but thin layering may be due to metamorphic differentiation. May show contacts discordant to layering in country rocks; may show relict igneous textures, cumulus layers, zoning in plagioclase phenocrysts, subophitic or ophitic textures; may contain relict minerals such as augite, hypersthene, or olivine; hornblende and plagioclase are subequal in abundance, + almandine + epidote + sphene + apatite + ilmenite and other opaques; + minor biotite, quartz, or diopside. Chemical trend, such as the MgO/(MgO + FeO) ratio in samples across the body, follows that for differentiation of diabase or gabbro; Cr, Ni may be high (250 ppm), as may Ti, Cu; Rb/Sr ratio is low (0.3–0.33). La/Ce ratio is low (< 0.4); high (+) ϵ_{Nd} (Wiseman, 1934; Walker and others, 1960; Engel and Engel, 1962a; Leake, 1963; Gates, 1967; Tobisch, 1968; Heimlich and Uthe, 1976; M. Perfit, personal communication, 1982; Cummings, 1984)
Metamorphism of basalt flow (see Fig. 11-14)	May show discordant lower contact unconformity; may show relict volcanic flow textures, zoning in plagioclase, phenocrysts, amygdules, monolithologic breccia, pillow structures; hornblende and plagioclase in subequal abundance, + almandine + epidote + sphene + apatite + opaques. Most commonly chemically equivalent to tholeiitic basalt but may be calc-alkaline; low oxidation ratio [$(2Fe_2O_3 \times 100)/(Fe_2O_3 + FeO)$] of about 30; Cr, Ni, high. High (+) ϵ_{Nd} (Engel and Engel, 1962b; Leake, 1963, 1964; Holdaway, 1965; Hurst and Jones, 1973; Barker and Peterman, 1974; Rivalenti, 1976; M. Perfit, personal communication, 1982)

Possible origin	Criteria used for determination
Metamorphism of basalt tuff or tuff mixed with carbonate	Constant composition, persistence along strike; layered, relict lapilli or agglomerate textures; tuffs of basalt composition forming thin persistent layers rare in unmetamorphosed sedimentary sequences. High oxidation ratio [$(2Fe_2O_3 \times 100)/(Fe_2O_3 + FeO)$ averages 68]; chemistry does not follow pelitic rock-carbonate trend. Intermediate $\pm$ ϵ_{Nd} (Evans and Leake, 1960; Engel and Engel, 1962; Holdaway, 1965; van de Kamp, 1970; M. Perfit, personal communication, 1982)
Metamorphism of shaly limestone or calcareous shale	Layered but not monotonously the same for tens of kilometers along strike and in successive beds for hundreds of meters across strike. Layering can probably also develop on a regional scale by metamorphic differentiation (Walker and others, 1960, p. 155, however, disagree); concordantly interlayered on a centimeter scale with marble, pelitic schist, and other clearly metasedimentary layers; widely varying mineral percentages; hornblende generally more abundant than plagioclase; biotite, quartz, diopside, or epidote may be abundant; sphene and apatite may be present; almandine is generally absent; the chemical trend of different samples lies at a large angle to the differentiation trend of basalt on CaO: MgO/MgO + FeO or on Al + alkalis; Mg/(Mg + Fe): CaO; K > Na; lower in Ni, Cr, Ti, Sc, Cu; negative correlation of Cr, Ni with Mg/(Mg + Fe): positive correlation of Ti with Mg/(Mg + Fe); higher in Ba, Pb, Au. Low (−) ϵ_{Nd} (Eckelmann and Poldervaart, 1957; Evans and Leake, 1960; Walker and others, 1960; Leake, 1963, 1964; M. Perfit, personal communication, 1982)
Metasomatic replacement of marble	Transition to parent carbonate rock from a rock of suitable composition; may have relict carbonate; marble parent makes sense in the parent stratigraphic sequence (Buddington, 1939; Engel and Engel, 1962)
Metasomatic replacement of pyroxene granulite (metasediment)	Pyroxene granulite adjacent to metagabbro; Sr 1000–1450 ppm in gabbroic plagioclase of composition An_{56-67}; Sr 250–900, with one 1100, ppm in metasomatic amphibolite plagioclase of composition An_{40-82} (Skiba and Butler, 1963)

TABLE 2: Summary of the Petrography of the SPMS amphibolite samples.

Sample #1: Near batholith. Contains plagioclase, highly-birefringent amphibole= hornblende, quartz that is pale tan under uncrossed nichols, large crystals of biotite, chlorite, "grunge", and lots of opaques such as pyrite and magnetite.

Sample #3: Near batholith. Contains some form of iron-staining from the opaques. No biotite found. Does possess large percentage of plagioclase (45%), highly-birifringent amphibole= hornblende, and "grunge".

Sample #6: Near batholith. Contains highly-birifringent amphiboles= hornblende that have brown-green pleochroism and near parallel extinction. Also has large crystals of plagioclase, small amount of quartz. No garnet seen. Contains long strands of biotite crystals: brown, highly pleochroic, and have high-birefringence.

Sample #10: Thompson Peak, near batholith. Contains biotite, quartz, plagioclase, hornblende, and opaques.

Sample #12: Top of Thompson Peak, near batholith. Contains 45% plagioclase, 35% amphiboles, "grunge", biotite, <10% quartz, and <10% opaques.

Sample #16: Leggat Cirque, near disturbed zone. Contains >10% opaques, <10% plagioclase, large amphiboles= hornblende, large grains of quartz, and "grunge".

Sample #21B: Contains plagioclase (Al50-An50), large opaques, large hornblende grains, and @ 10% quartz.

Sample #22A: Contains large, altered-looking hornblende grains. Also, possesses large crystals of plagioclase, large quartz crystals that show undulatory extinction, @ 10% opaques, and a large amount of garnet.

Sample #24A: Contains large grains of quartz, a large amount of "grunge", plagioclase, opaques that are probably magnetite, and <5% biotite.

Sample #24D: Leggat Cirque, near disturbed zone. Contains 20% plagioclase (Al65-An35), @ 50% garnet, a large vein of quartz, "grunge", muscovite, amphibole= hornblende (25-30%), and quartz crystals (15%).

Sample #25: Contains lots of "grunge", large plagioclase crystals (Al35-An65), garnet, opaques= pyrite, large, euhedral crystals of hornblende, large quartz crystals in vein, and small quartz crystals elsewhere in section.

Sample #28B: Contains amphiboles= mainly hornblende (riebeckite=2%), opaques, garnet, plagioclase (Al90-An10), and quartz.

Sample #29D: Contains large plagioclase grains (Al>90-An10), "solution cracks", large grains of amphibole= hornblende, opaques, and quartz (<3%).

Sample #30: Contains quartz (<10%), plagioclase (Al87-An13), hornblende, and opaques.

Sample #31: Leggat Ridge, near contact with ICMS. Fine-grained. Contains <10% opaques, 15-20% garnet, plagioclase (Al85-An15 to Al95-An5), 10-15% quartz, hornblende, and "grunge".

Sample #31B: Leggat Ridge, near contact with ICMS. Fine-grained. Contains biotite (10%), garnet, amphiboles= hornblende and cummingtonite or riebeckite, and plagioclase (Al85-An15).

Sample #31C: Leggat Ridge, near contact with ICMS. Contains garnet, amphibole= hornblende, plagioclase (Al90-An10), and 20% quartz.

Sample #34E: Shows a distinct mineral lineation, especially in the amphiboles= hornblende. Contains garnet, opaques, 25% quartz, and 20% plagioclase (Al50-An50).

Sample #35A: Contains >5% biotite, amphibole= hornblende, plagioclase (Al90-An10), quartz (<10%), and "grunge" with garnets.

Sample #39C: Contains large opaques, 15-20% quartz, amphiboles= hornblende (50-60%), and 30-40% plagioclase (Al45-An55).

Sample #40C: Contains about 25% plagioclase (Al55-An45), a large amount of "grunge", <5% quartz, >70% hornblende, opaques, and garnet.

Sample #40D: Contains about 30% plagioclase (Al65-An35), "grunge" with opaques, 15-20% quartz, 65% hornblende, 5% accessory minerals (opaques), and no real evidence of garnet.

Sample #41: Contains very large crystals of quartz, large amounts of "grunge" with garnets (broken), amphiboles = hornblende predominately with some cummingtonite, biotite, and @ 10% plagioclase (Al65-An35).

Sample #42: Thompson Ridge-meadow area-near batholith. Contains 25% plagioclase (Al55-An45), large amounts of "grunge", holed amphiboles =hornblende, opaques, some large crystals of quartz (15%), and 5% biotite.

Sample #A_D (Amphibolite-Disturbed Zone): Disturbed zone area. Contains 2-3% opaques, broken garnets surrounded by "grunge", amphiboles= hornblende, >15% quartz, very little plagioclase, biotite, and chlorite.

Table 3: XRF Analyses of major and trace element geochemistry for selected samples from the SPMS amphibolites											
	Sample 1	Sample 3	Sample 6	Sample 10	Sample 12	Sample 16	Sample 21B	Sample 22A	Sample 24A	Sample 24D	Sample 25
(wt. %)											
SiO2	48.173	48.4	46.7	56.771	56.1	51.732	51.638	50.357	50.14	48.7	52.4
Al2O3	13.76	13	17	14.473	12.9	13.106	15.191	17.783	14.59	16.8	13
Cr2O3	0.018036	<0.01	0.1	0.016213	0.05	0.012738	0.04398	0.0084365	0.021761	<0.01	<0.01
FeO	7.303	6.749	3.811	4.983	4.373	7.565	4.118	4.56	5.884	7.693	7.558
Fe2O3	16.232	15	8.47	11.076	9.72	16.814	9.152	10.136	13.078	17.1	16.8
MnO	0.417	0.26	0.25	0.168	0.17	0.299	0.231	0.233	0.294	1.08	0.32
MgO	6.747	7.17	9.94	5.233	7.84	5.896	8.378	6.528	6.721	4.11	4.96
CaO	10.055	10.2	10.6	8.227	7.73	9.465	12.552	11.935	9.369	6.45	7.07
Na2O	2.04	2.21	1.98	2.809	2.43	0.613	1.212	2.459	3.191	1.76	1.34
K2O	0.506	0.9	0.56	0.547	0.21	0.902	0.28	0.208	0.993	0.57	0.51
P2O5	0.115	0.09	<0.01	0.139	0.07	0.095	0.034	0.032	0.091	0.25	0.15
TiO2	1.328	1.26	0.36	0.764	0.53	1.429	0.641	0.502	0.847	1.71	1.86
LOI	0.6	0.75	1.2	0.7013	0.3	0.738	0.9966	0.4426	0.75	0.25	0.2
SUM	99.973	99.29	97.21	100.9083	98.09	101.089	100.3056	100.6156	100.064	98.83	98.65
(ppm)											
Ba		60	230		80					130	100
Cr	123.366	<68.4	684	110.895	342	87.129	300.823	57.706	148.842	<68.4	<68.4
Cu	171.795			86.43		221.838	132.234	91.596	90.978		
Ga	19.405			15.749		10.185	14.22	15.964	17.824		
Nb	5.253	6	<2	4.956	3	1.317	0.912	0.701	4.505	13	7
Ni	91.037			62.473		58.077	94.617	44.957	97.22		
Rb	17.492	42	9	7.64	<2	13.545	6.232	2.332	15.59	2	12
Sr	114.126	174	139	155.656	124	47.59	139.516	156.095	123.954	85	95
Th	3.82			6.304		2.243	2.099	1.296	2.156		
Ti	7961.36	7553.7	2158.2	4580.18	3177.35	8566.855	3842.795	3009.49	5077.77	10251.45	11150.7
U	1.103			1.747		0.136	0.473	0.449	1.359		
V	316.199			191.32		383.47	210.19	169.191	263.198		
Y	37.331	29	4	26.942	17	33.552	17.941	12.989	24.259	37	29
Zn	94.72			85.928		113.894	69.996	82.665	98.606		
Zr	113.818	79	31	129.834	78	92.342	38.314	31.762	56.032	130	120

Table 3 (cont.)

	Sample 26	Sample 28B	Sample 29D	Sample 30E	Sample 31	Sample 31B	Sample 31C	Sample 32	Sample 33D	Sample 34E	Sample 35A
(wt. %)											(wt. %)
SiO2	51.426	49.5	46.4	48.8	48.373	55.1	52.214	51.244	44.463	49.7	49
Al2O3	13.894	15.9	17.5	14	13.492	14	15.471	8.275	19.498	13.8	13.6
Cr2O3	0.01598	0.03	0.12	<0.01	0.0064996	<0.01	0.014435	0.17664	0.034608	<0.01	0.01
FeO	6.583	4.252	3.946	6.209	8.535	4.949	5.16	6.75	4.23	6.614	6.884
Fe2O3	14.631	9.45	8.77	13.8	18.971	11	11.468	15.002	9.402	14.7	15.3
MnO	0.197	0.24	0.23	0.55	0.677	0.2	0.289	0.552	0.216	0.24	0.21
MgO	6.431	7.44	9.67	6.88	5.001	5.16	6.64	15.626	10.928	6.32	6.49
CaO	8.96	10.7	12.4	9.57	9.379	7.8	10.367	6.772	11.211	9.68	9.71
Na2O	1.924	2.06	1.29	2.65	1.945	3.04	1.812	1.018	1.508	1.38	1.15
K2O	0.725	0.48	0.27	0.58	0.57	0.65	0.484	0.137	0.408	0.7	0.97
P2O5	0.101	0.06	0.03	0.08	0.063	0.15	0.042	0.068	0.015	0.11	0.13
TiO2	1.159	0.81	0.39	0.91	1.515	0.77	0.683	0.502	0.288	1.14	1.06
LOI	0.6454	0.95	0.65	0.3	0.3471	0.4	0.6778	1.065	1.689	0.5	0.45
SUM	100.0934	97.66	97.75	98.16	100.3331	98.34	100.1478	100.261	99.626	98.31	98.12
(ppm)											(ppm)
Ba		140	50	120		240				70	140
Cr	109.304	205.2	820.8	<68.4	44.457	<68.4	98.734	1208.214	236.718	<68.4	68.4
Cu	80.044				78.103		93.863	63.467	15.408		
Ga	17.673				19.793		16.172	9.412	13.684		
Nb	4.835	3	<2	12	1.571	6	1.27	0.579	-0.158	6	<2
Ni	82.609				63.548		80.337	215.676	324.775		
Rb	11.006	4	8	4	6.976	<2	6.753	2.384	12.827	4	8
Sr	106.356	161	119	123	112.45	162	212.915	14.065	136.597	104	91
Th	4.603				2.082		3.541	2.015	1.472		
Ti	6948.205	4855.95	2338.05	5455.45	9082.425	4616.15	4094.585	3009.49	1726.56	6834.3	6354.7
U	0.386				1.737		-0.047	0.011	0.469		
V	295.541				1142.104		389.274	156.337	81.493		
Y	29.559	11	5	16	23.257	22	14.06	13.224	8.158	25	17
Zn	110.721				91.503		74.756	103.883	85.213		
Zr	102.832	53	28	57	71.64	130	49.797	37.159	21.471	100	69

Table 3 (cont.)

	Sample 36B	Sample 37B	Sample 38A	Sample 39C	Sample 40C	Sample 40D	Sample 41	Sample 42	Sample AmDis
(wt. %)									
SiO2	58.757	52.9	49.3	51.429	49.7	50.685	50.436	49.637	49.914
Al2O3	14.205	14.7	12.9	13.422	13.8	14.544	15.174	13.941	13.372
Cr2O3	0.028071	0.05	<0.01	0.02319	<0.01	0.012656	0.037487	0.022042	0.01582
FeO	4.278	4.634	7.693	5.78	6.929	6.501	6.265	6.933	7.725
Fe2O3	9.508	10.3	17.1	12.846	15.4	14.45	13.924	15.41	17.17
MnO	0.15	0.17	0.25	0.211	0.22	0.216	0.227	0.215	0.334
MgO	5.946	6.99	5.02	7.816	6.23	5.648	7.234	6.962	5.972
CaO	6.973	8.22	8.13	11.344	10.3	9.842	9.18	10.731	9.774
Na2O	2.748	2.38	3.13	1.535	1.46	2.09	1.293	1.166	0.702
K2O	0.458	1.46	0.46	0.244	0.32	0.451	0.349	0.25	0.832
P2O5	0.108	0.07	0.19	0.042	0.15	0.127	0.078	0.096	0.105
TiO2	0.717	0.65	1.93	0.54	1.64	1.485	1.058	1.135	1.505
LOI	0.627	0.8	0.28	0.9744	0.2	0.8491	1.15	0.6796	0.7786
SUM	100.197	98.77	98.74	100.4034	99.46	100.3871	100.103	100.2226	100.4586
(ppm)									
Ba		370	70		50				
Cr	192.006	342	<68.4	158.623	<68.4	86.57	256.414	150.766	72.384
Cu	24.957			229.379		72.418	216.898	152.942	184.07
Ga	16.958			13.3		18.593	17.43	18.084	18.977
Nb	7.58	2	7	0.831	9	5.897	1.766	4.354	0.672
Ni	152.335			97.423		61.057	87.128	99.659	53.868
Rb	11.71	41	12	6.565	3	9.13	6.575	6.341	17.173
Sr	326.501	152	103	85.571	150	149.814	142.438	95.413	54.351
Th	12.643			2.948		2.319	1.226	1.775	1.05
Ti	4298.415	3896.75	11570.35	3237.3	9831.8	8902.575	6342.71	6804.325	9022.475
U	3.315			-0.22		-0.337	0.82	1.775	-0.809
V	147.675			219.331		298.292	263.799	317.133	410.17
Y	36.014	23	39	15.614	27	29.589	25.017	30.004	35.023
Zn	78.369			88.765		109.329	92.347	118.96	135.925
Zr	186.262	92	140	36.357	120	99.907	82.101	86.903	90.269

Table 4: Rare-earth-element data (ppm) for amphibolites of the SPMS								
REE	Sample 1	Sample 3	Sample 6	Sample 10	Sample 12	Sample 16	Sample 21B	Sample 22A
La	14.2	3.8	1.7	19.5	14.1	2.5	3.1	3.3
Ce	29.5	12.7	4.9	37.8	24	7.3	8.5	7
Nd	12	6.3	1	17	11.6	4.8	1.3	4.7
Sm	4.7	3.5	0.82	4	2.6	2.1	1.9	1.4
Gd	0.67	0.29	0.09	0.7	0.41	0.37	0.4	0.14
Yb	3.6	1.1	0.72	2.7	1.8	2.2	1.5	1.3
Lu	0.52	0.2	0.09	0.32	0.25	0.31	0.21	0.19
REE	Sample 24A	Sample 24D	Sample 25	Sample 26	Sample 28B	Sample 29D	Sample 30E	Sample 31
La	7.3	10.5	13.6	9.7	4	1.8	5.1	14.3
Ce	14.7	22.2	29.7	19.4	8.3	5.4	12.6	22.8
Nd	8.5	13.4	13.2	5.5	4.9	0.9	5.3	9.7
Sm	2.6	4.4	4.8	3.2	1.7	0.92	2.6	2.4
Gd	0.28	0.42	0.48	0.48	0.07	0.1	0.17	0.32
Yb	1.9	4	3.4	2.4	1.42	0.88	2.2	1.7
Lu	0.27	0.57	0.42	0.35	0.21	0.11	0.29	0.26

Table 5: Niggli Values for selected samples from the SPMS amphibolites											
Niggli value	Sample 1	Sample 3	Sample 6	Sample 10	Sample 12	Sample 16	Sample 21B	Sample 22A	Sample 24A	Sample 24D	Sample 25
al	18.4754047	17.5743175	22.1709484	23.2019394	20.208962	18.9301616	20.607654	24.130297	20.2032812	25.4955219	20.5825477
fm	51.6904995	51.0744876	47.6084555	44.4155338	51.1142748	53.298469	45.2605894	40.5760685	47.4047461	51.3426937	54.6623148
c	24.5906351	25.1158241	25.1798628	24.0225645	22.0569742	24.9010077	31.0146772	29.4979752	23.6304504	17.8289794	20.3885968
alk	5.24346065	6.23537082	5.04073326	8.35996232	6.61978901	2.8703617	3.11707931	5.79565924	8.76152234	5.33280499	4.36654061
mg	0.44690549	0.48393879	0.69434901	0.48163912	0.61272886	0.40744321	0.64032804	0.55668305	0.5006323	0.30978328	0.36634445
k	0.14059839	0.21173256	0.1572179	0.11382065	0.05392644	0.49252285	0.13222838	0.05284336	0.17029763	0.17601355	0.20065998
	Sample 26	Sample 28B	Sample 29D	Sample 30E	Sample 31	Sample 31B	Sample 31C	Sample 32	Sample 33D	Sample 34E	
al	19.9910115	22.5008493	22.2445613	19.3509592	18.6601193	22.8077442	22.1558665	10.0670646	23.490251	19.8095988	
fm	50.8411727	44.3858693	45.976285	49.659709	52.4320089	44.7502722	45.7811049	72.7086463	48.3864292	50.5315191	
c	23.4815969	27.5802189	28.7091032	24.0934252	23.6269012	23.1452057	27.0418001	15.0059657	24.6010752	25.3095309	
alk	5.68621897	5.5330626	3.07005045	6.89590662	5.28097054	9.2967778	5.02122845	2.21832334	3.52224451	4.34935109	
mg	0.46409897	0.60488132	0.68173968	0.4883137	0.33638655	0.47901432	0.52965411	0.66670973	0.69383289	0.45781656	
k	0.19906468	0.13321397	0.12130435	0.12614888	0.16198377	0.12359688	0.14978836	0.08152727	0.15142953	0.25069316	
	Sample 35A	Sample 36B	Sample 37B	Sample 38A	Sample 39C	Sample 40C	Sample 40D	Sample 41	Sample 42	Sample AmDis	
al	19.2667763	23.904746	22.1479969	18.8826894	18.2647136	19.3967271	20.9168059	21.3943133	18.9973594	18.8788966	
fm	51.5064305	46.2775065	47.0077052	51.1732909	49.8211977	50.3698421	47.6529463	51.4974676	51.3840325	53.0817987	
c	25.0554104	21.3734537	22.5580254	21.6758846	28.1173246	26.3693083	25.7814302	23.5750758	26.6349357	25.13418	
alk	4.1713827	8.4442938	8.28627255	8.26813507	3.79676412	3.86412254	5.64881767	3.53314335	2.9836724	2.90512468	
mg	0.4551909	0.55136352	0.57130158	0.3661632	0.54438506	0.44330947	0.43466694	0.50504617	0.47080962	0.4050369	
k	0.35746553	0.09904153	0.28806008	0.08836835	0.09489518	0.12630507	0.12459563	0.15112446	0.12389692	0.43874392	

Table 6: Y/Nb Ratios used in determining petrologic character (Pearce and Cann,1973).
Y/Nb for alkalic basalts is less than 1 for within-plate basalts and less than 2 for ocean-floor basalts. Y/Nb for tholeiitic rocks is greater than 2 for within-plate basalts and greater than 3 for ocean-floor basalts.
Except for sample #33, most of the SPMS amphibolites have a Y/Nb ratio greater than 3.

SAMPLE #	Y PPM	Nb PPM	Y/Nb
Sample 1	37.331	5.253	7.10660575
Sample 10	26.942	4.956	5.4362389
Sample 12	17	3	5.66666667
Sample 16	33.552	1.317	25.476082
Sample 21B	17.941	0.912	19.6721491
Sample 22A	12.989	0.701	18.5292439
Sample 24A	24.259	4.505	5.38490566
Sample 24D	37	13	2.84615385
Sample 25	29	7	4.14285714
Sample 26	29.559	4.835	6.11354705
Sample 28B	11	3	3.66666667
Sample 29D	5	1.9	2.63157895
Sample 3	29	6	4.83333333
Sample 30E	16	12	1.33333333
Sample 31	23.257	1.571	14.8039465
Sample 31B	22	6	3.66666667
Sample 31C	14.06	1.27	11.0708661
Sample 32	13.224	0.579	22.8393782
Sample 33D	8.158	-0.158	-51.6329114
Sample 34E	25	6	4.16666667
Sample 35A	17	1.9	8.94736842
Sample 36B	36.014	7.58	4.75118734
Sample 37B	23	2	11.5
Sample 38A	39	7	5.57142857
Sample 39C	15.614	0.831	18.7894103
Sample 40C	27	9	3
Sample 40D	29.589	5.897	5.01763609
Sample 41	25.017	1.766	14.1659117
Sample 42	30.004	4.354	6.89113459
Sample 6	4	1.9	2.10526316
Sample AmDis	35.023	0.672	52.1175595

Table 7: Tectonic Discriminant Diagram Summary							
	Diagram						
Environment	Mullen	Meschede	MgO-FeO-AlO	Zr-Ti Diag.	Zr-Ti-Sr	Zr-Ti-Y	Ti-Cr Diag.
OceanFloorBasalts		4	3	18	13	24	9
IslandArcBasalts	14	26	20	12	5	19	11
CalcAlkaliBasalts	13	4		4	7	5	
ContinentalBasalts			6				
WtihinPlateBasalts		1				4	
MOR Basalts	1	26	3				

Table 7: A summary of the distribution of the SPMS amphibolites plotted on 7 different tectonic discriminant diagrams. Some overlap occurs on the diagrams as distinguishing between tectonic environments can prove impossible using certain major and trace elements. The majority of SPMS amphibolites plot as ocean-floor basalts on Pearce and Cann (1973) diagrams. Meschede does not separate the field for island-arc basalts and MORB's on the Nb-Zr-Y plot, so 26 samples are included for both categories. The SPMS amphibolites plot mainly as island-arc basalts on the MgO-FeO-AlO diagram (Pearce et al., 1977). One should note that these parameters are major elements, which many times are mobile during metamorphic events.

Table 8: Tectonic Environments-Summary of Graph Findings						
	Mullen 83	Pearce/Sr/2 73	Meschede 86	Pearce/Y*3 73	ZR-TI Diag	PrceMgFeAL
Sample 1	CAB	Ocean Floor	NMORB,VAB	IAB, Ocean Floor	OFB	OceanIsland
Sample 6		CAB		Withn Plate	LowKThol	OceanRidge
Sample 10	IAT	CAB	PMORB,VAB	CAB, Ocean Floor	CAB	Continental
Sample 12		CAB	PMORB,VAB	CAB, Ocean Floor	CAB	OceanIsland
Sample 16	IAT	outsidebounds	NMORB,VAB		OFB	OceanIsland
Sample 21B	CAB	IABasalt	NMORB,VAB	IAB, Ocean Floor	OFB, LowKThol	OceanIsland
Sample 22A	CAB	IABasalt	NMORB,VAB	IAB, Ocean Floor	LowKThol	Continental
Sample 24A	CAB	Ocean Floor	OFB,LowKTh,CAB		OFB, LowKThol	OceanIsland
Sample 24D	CAB	outsidebounds	OFB,LowKTh,CAB	IAB, Ocean Floor	OFB	
Sample 25	IAT	Ocean Floor	PMORB,VAB	WithnPlateBaslt	Ocean Floor	OceanIsland
Sample 26	IAT	Ocean Floor	NMORB,VAB	IAB, Ocean Floor	OFB	OceanIsland
Sample 28B	CAB	IABasalt	PMORB,VAB	Withn Plate	OFB, LowKThol	OceanIsland
Sample 29D	CAB	IABasalt		Withn Plate	LowKThol	OceanRidge
Sample 3	IAT	Ocean Floor	OFB,LowKTh,CAB		OFB	OceanIsland
Sample 30E	CAB	Ocean Floor	WithnPlateThol	OceanFloor/IAB	OFB,LowKThol	OceanIsland
Sample 31	CAB		NMORB,VAB	IAB, Ocean Floor	outside bounds	OceanIsland
Sample 31B		CAB	PMORB,VAB	CAB, Ocean Floor	CAB	Continental
Sample 31C	CAB	IABasalt	NMORB,VAB	IAB, Ocean Floor	OFB, LowKThol	Continental
Sample 32	CAB	outsidebounds	NMORB,VAB	IAB, Ocean Floor	LowKThol	OceanIsland
Sample 33D	CAB	CAB	close to NMORB	IAB, Ocean Floor	LowKThol	OceanRidge
Sample 34E	IAT		PMORB,VAB	IAB, Ocean Floor	OFB	OceanIsland
Sample 35A	IAT	Ocean Floor		IAB, Ocean Floor	OFB, LowKThol	OceanIsland
Sample 36B	IAT	CAB	PMORB,VAB	CAB, Ocean Floor	outsidebounds	Continental
Sample 37B	IsArcTHOL	CAB	NMORB,VAB	CAB, OceanFloor	CAB	OceanIsland
Sample 38A	MORB	Ocean Floor	NMORB,VAB	OceanFloor/IAB	Ocean Floor	OceanIsland
Sample 39C	CAB	Ocean Floor	NMORB,VAB	IAB, Ocean Floor	LowKThol	OceanIsland
Sample 40C	IAT	Ocean Floor	OFB,LowKTh,CAB	IAB, Ocean Floor	OFB	OceanIsland
Sample 40D	IAT	Ocean Floor	NMORB,VAB	IAB, Ocean Floor	OFB	Continental
Sample 41	IAT	Ocean Floor	NMORB,VAB	IAB, Ocean Floor	OFB	OceanIsland
Sample 42	IAT	Ocean Floor	NMORB,VAB	IAB, Ocean Floor	OFB	OceanIsland
Sample AmDis	IAT	outsidebounds	NMORB,VAB	IAB, Ocean Floor	OFB	

APPENDIX B: FIGURES

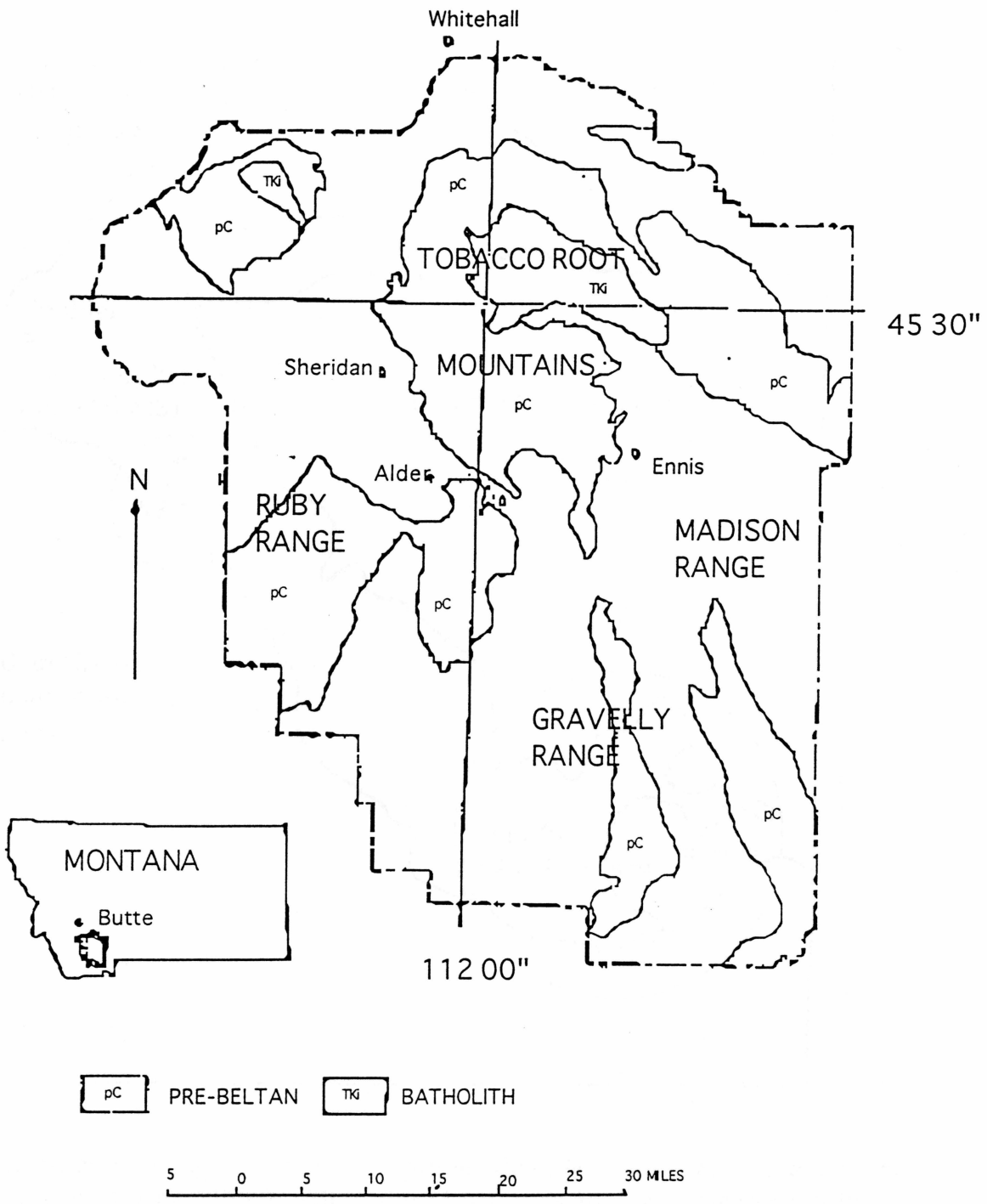

Figure 1: Map of Madison County, Montana, highlighting the location of the Tobacco Root Mountains in relation to neighboring ranges. Note the Pre-Beltan rocks that comprise the core of nearly all the ranges. (Cordua, 1973)

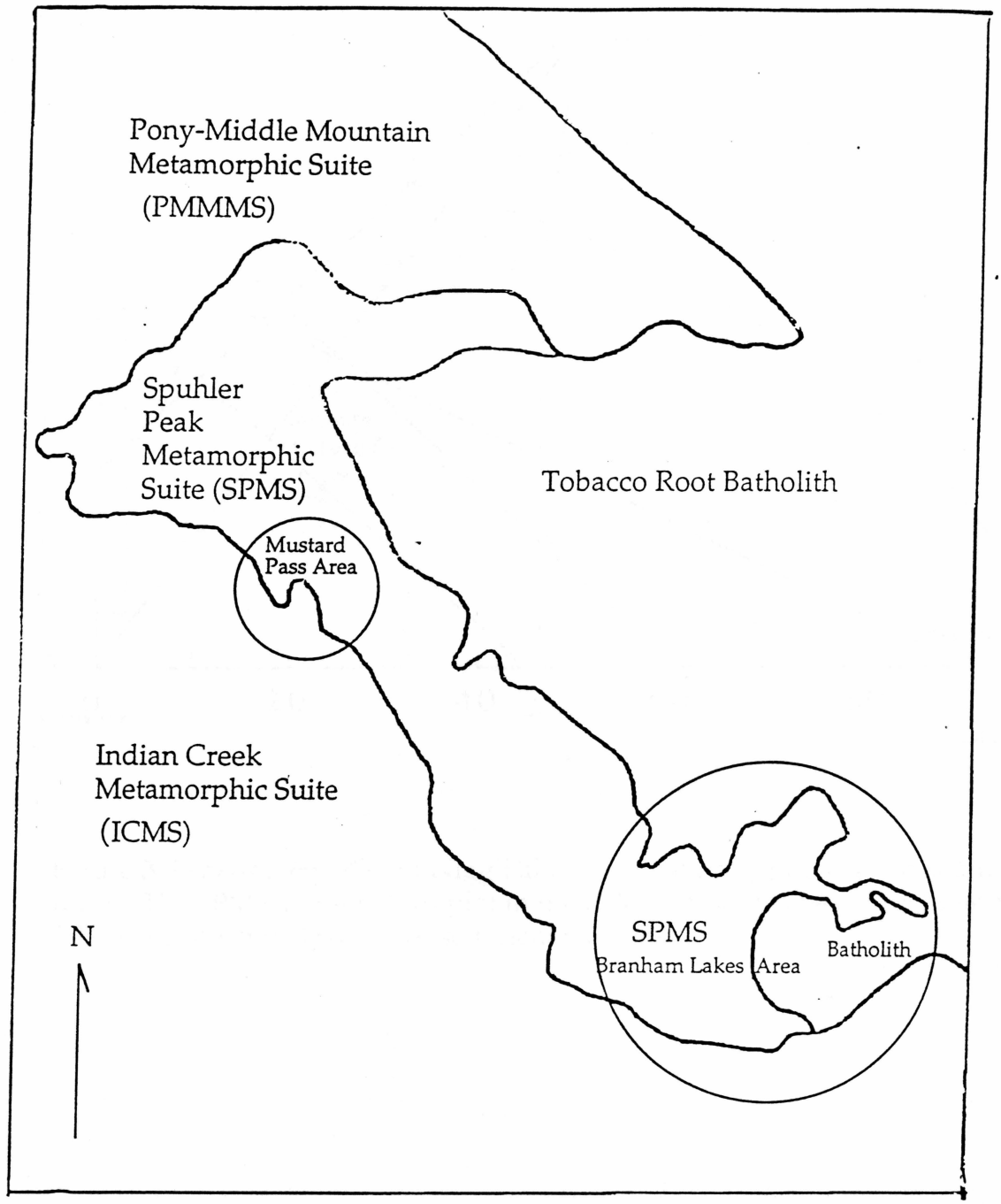

Figure 2: Generalized geologic map of the Spuhler Peak Metamorphic Suite and its neighbors in contact (Burger, 1969). All of the 31 samples analyzed for this study come from the SPMS in the Branham Lakes (28) and Mustard Pass (3) areas.

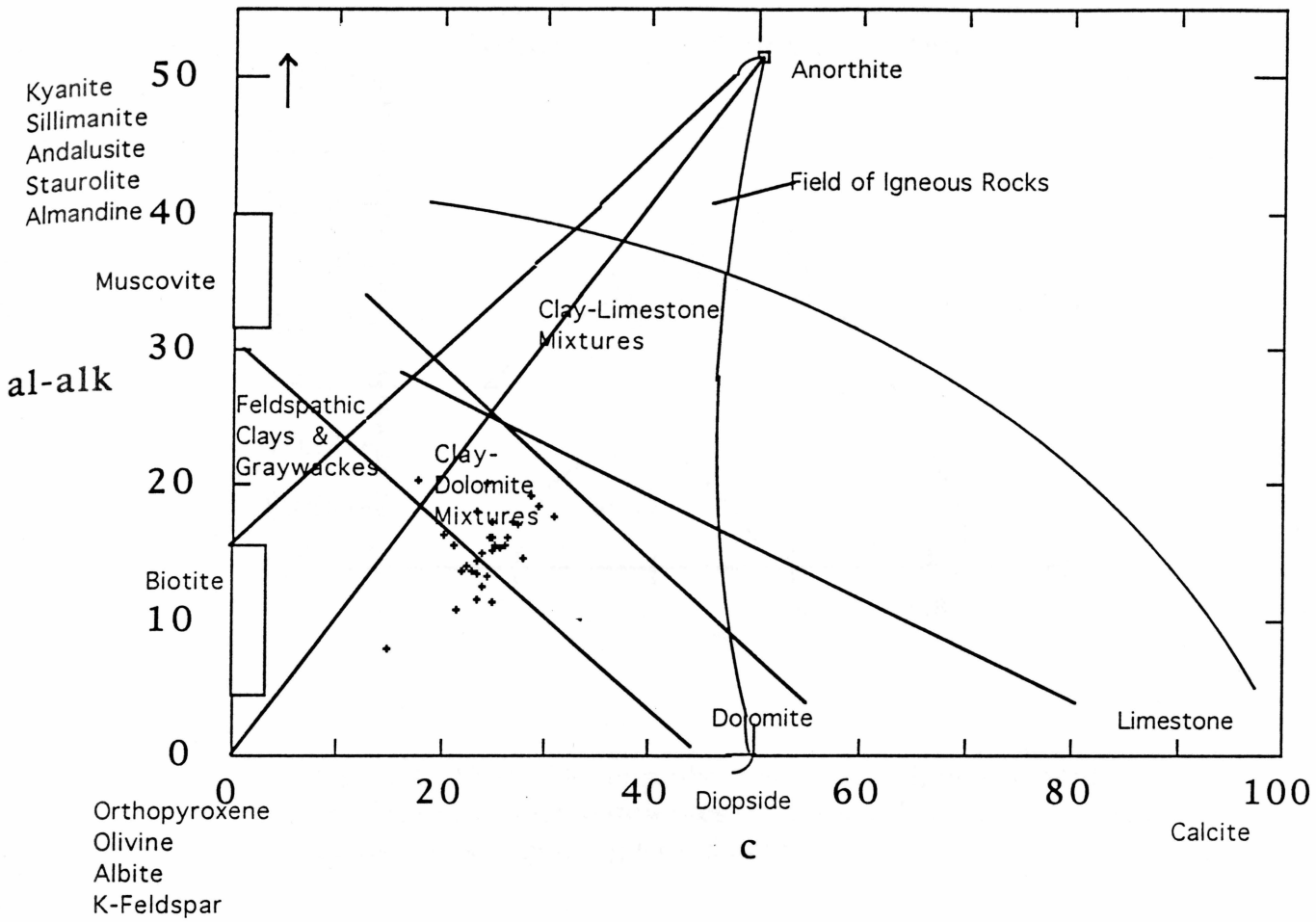

Figure 3: Leake (1969): Plot of Niggli al-alk against c for igneous and sedimentary rocks. The SPMS amphibolites plot in the fields for both types of rocks and do not follow a distinctive igneous or sedimentary trend.

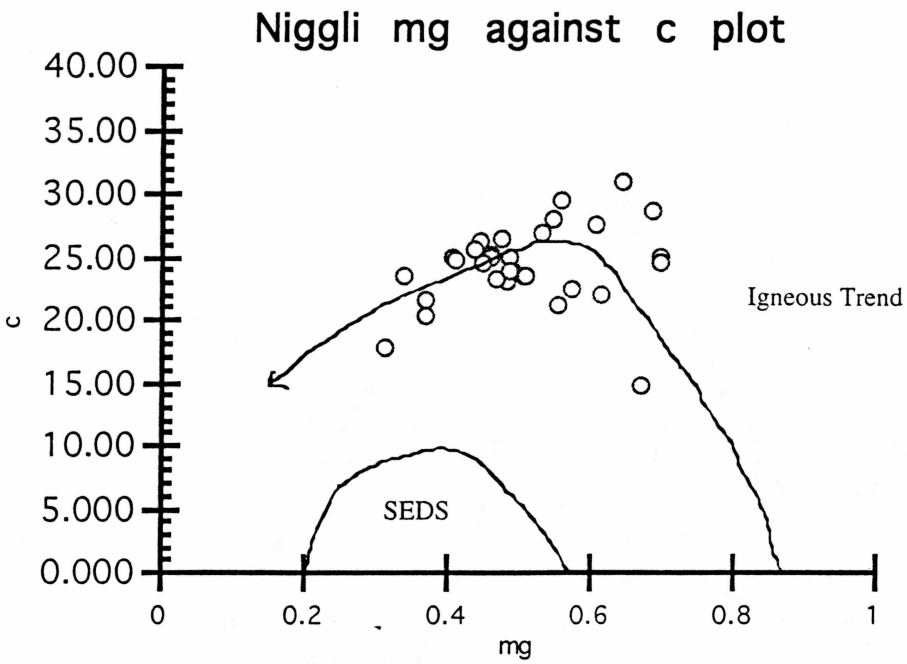

Figure 4: The SPMS amphibolites show an igneous trend similar to the Karroo dolerites (Evans and Leake, 1960) when plotted on a Niggli mg vs. c diagram.

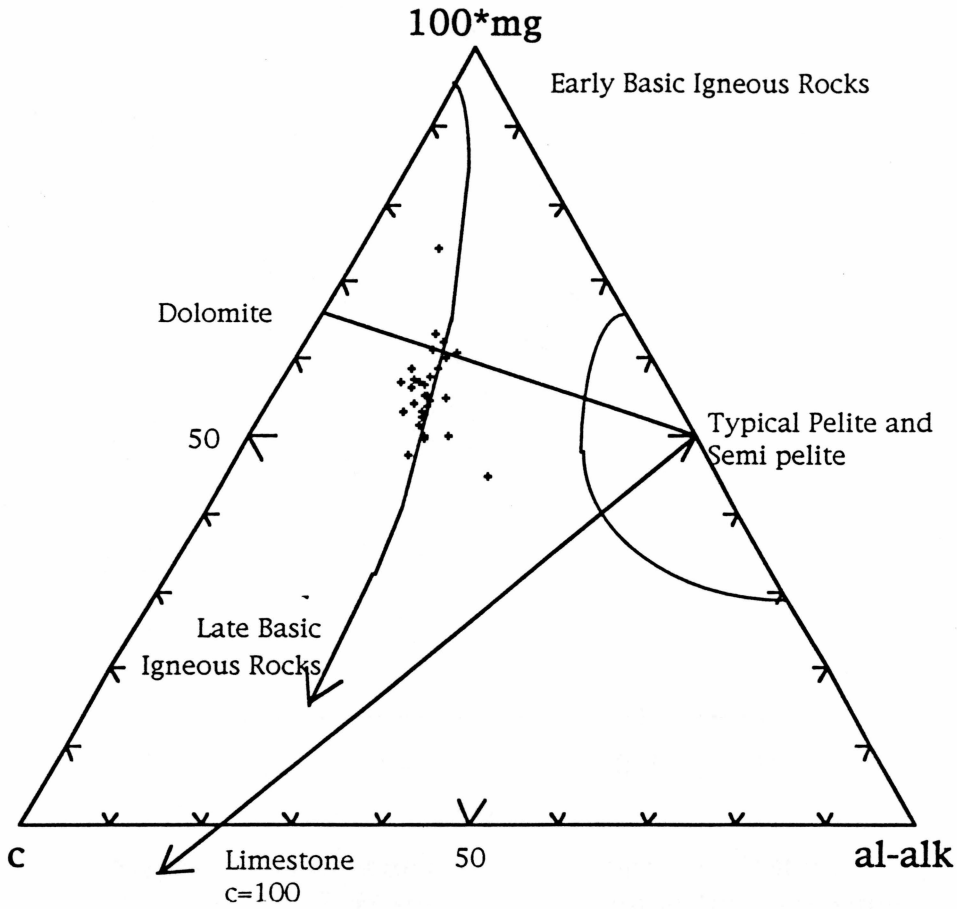

Figure 5: The SPMS amphibolites follow the trend from early basic to late igneous rocks when plotted on a 100*mg+c+(al-alk) diagram (Leake, 1963).

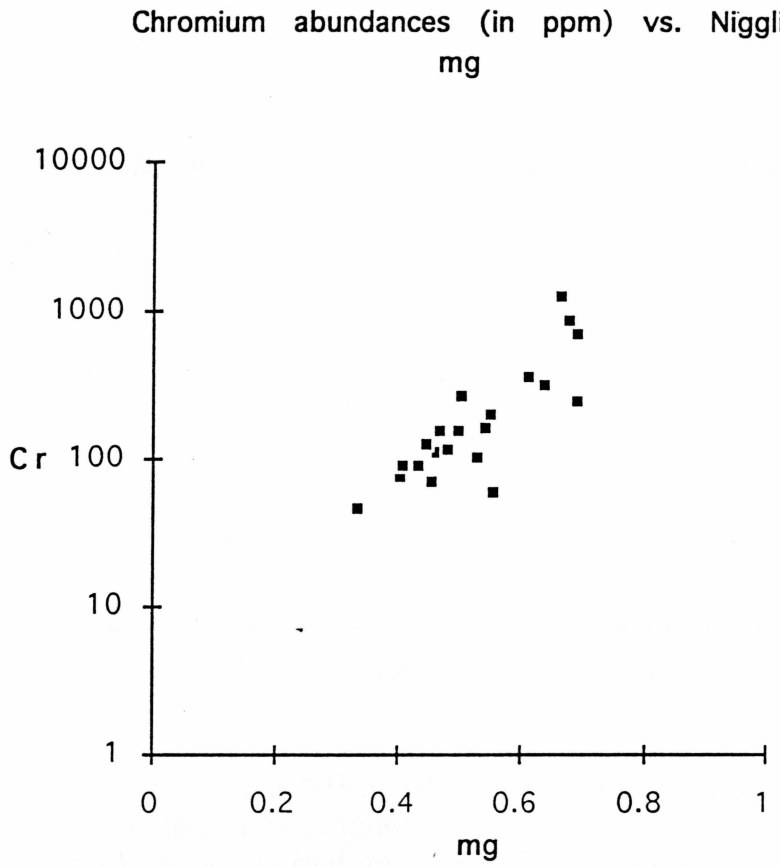

Figure 6: When plotted on a Cr (in ppm) against mg diagram, the SPMS amphibolites demonstrate a positive slope indicative of igneous rocks but not shale-carbonate rocks.

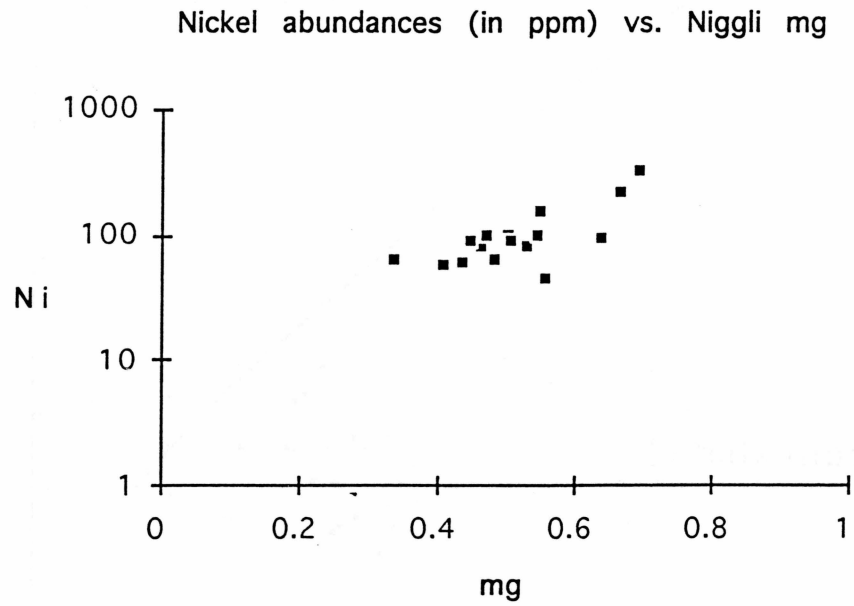

Figure 7: The SPMS amphibolites show positive correlations indicative of basic igneous rocks but not shale-carbonate rocks when plotted on a Ni vs. Niggli mg diagram.

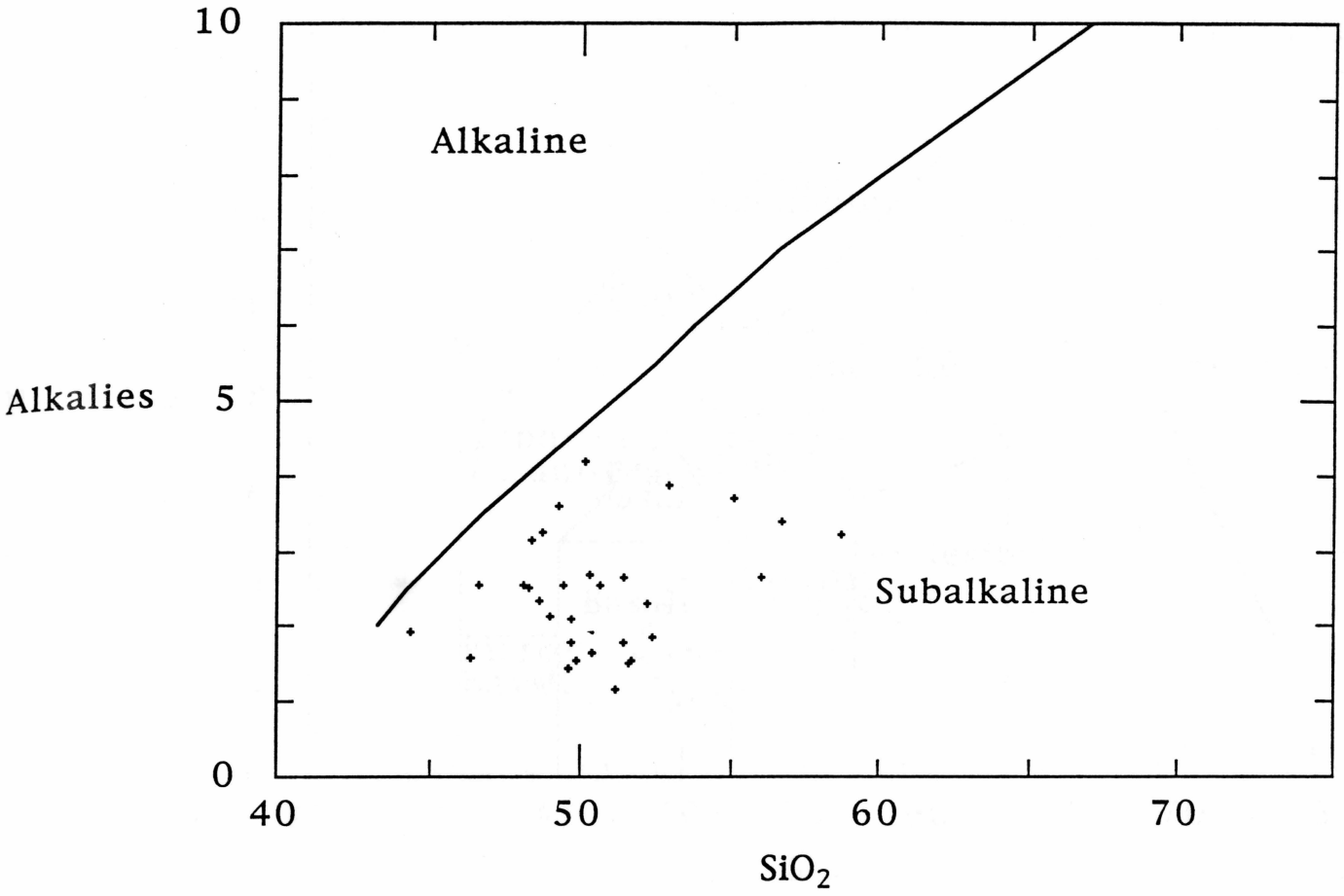

Figure 8: All of the SPMS amphibolites plot as subalkaline on the plot of SiO2 vs. (Na2O+K2O) or Alkalies.

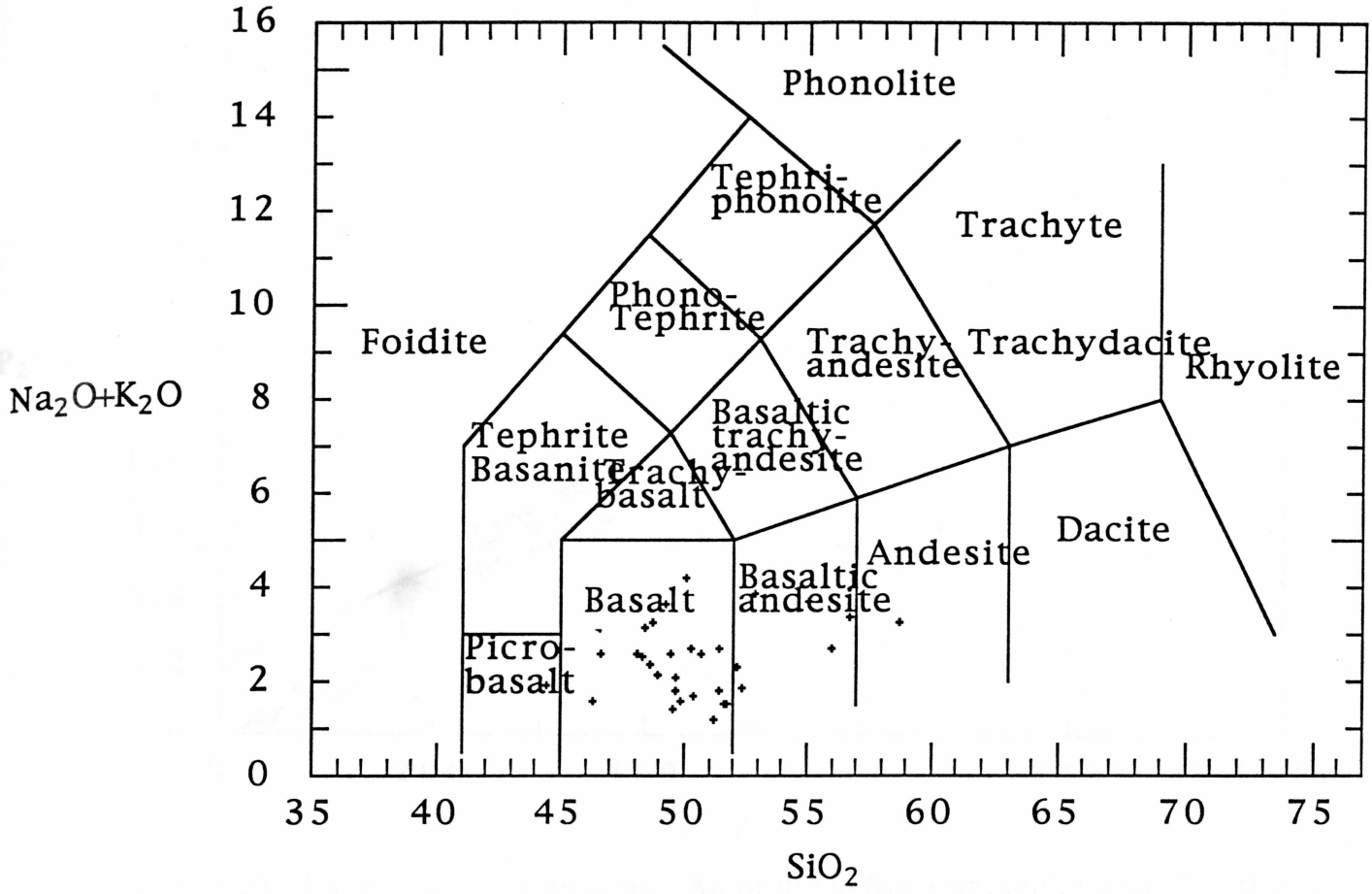

Figure 9: The SPMS amphibolites plot as modern-day picro-basalts, basalts, basalt andesites, and andesites on the total alkali-silica diagram (LeBas et al., 1986).

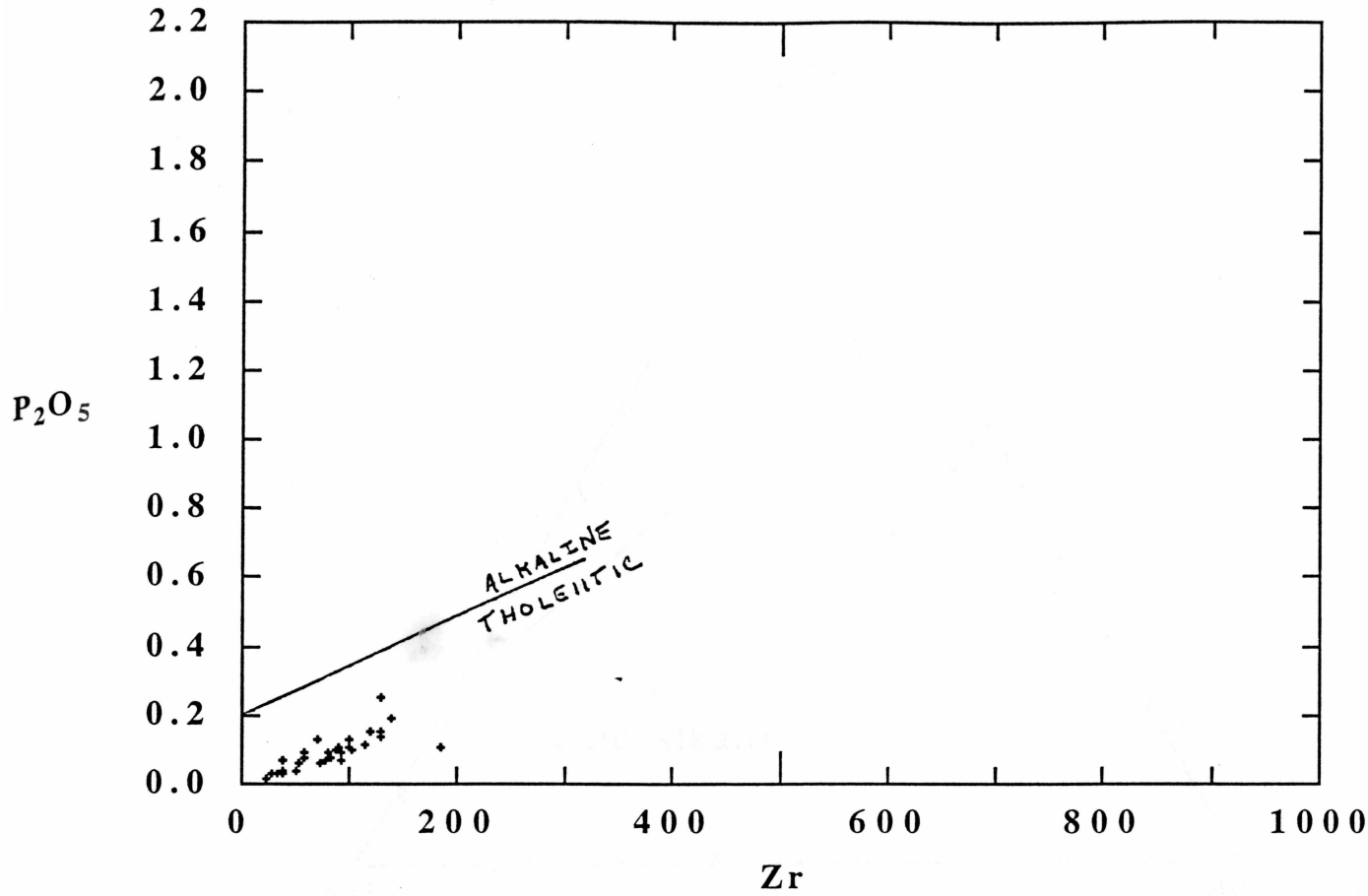

Figure 10: The Zr vs. P2O5 diagram. All of the SPMS amphibolite samples plot as tholeiitic and not alkaline.

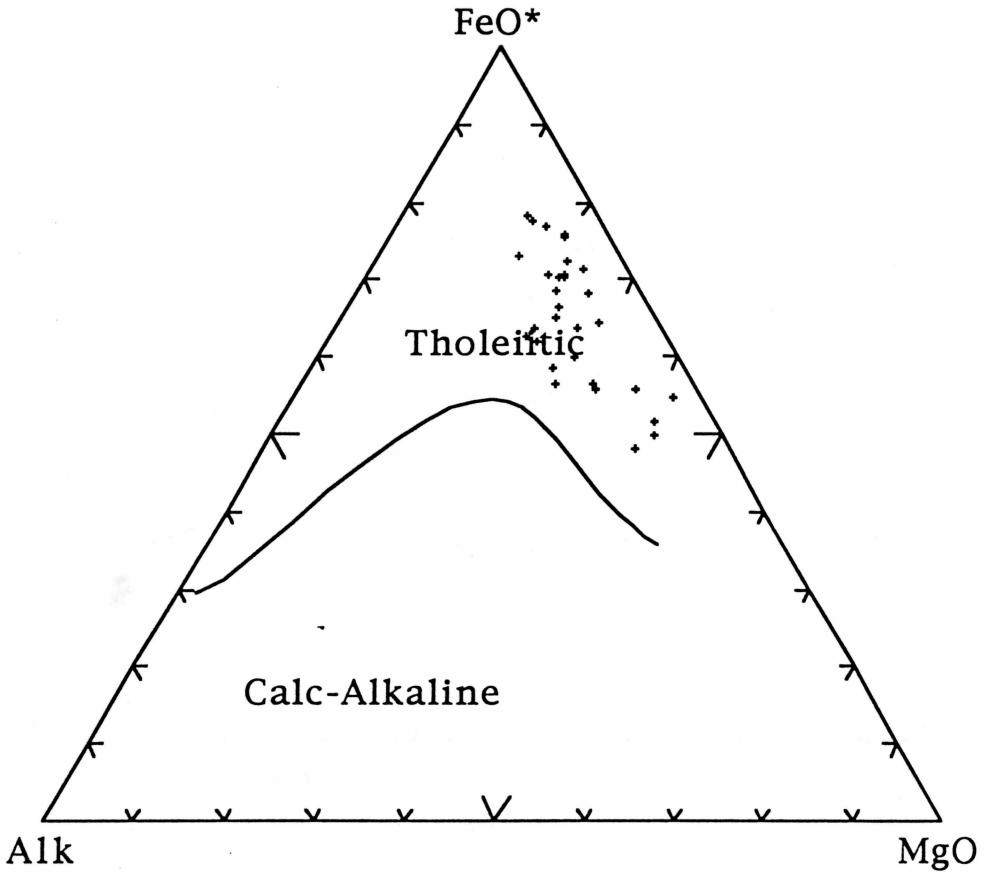

Figure 11: All samples of the SPMS amphibolites plot in the field of Tholeiitic basalts on the AFM diagram.

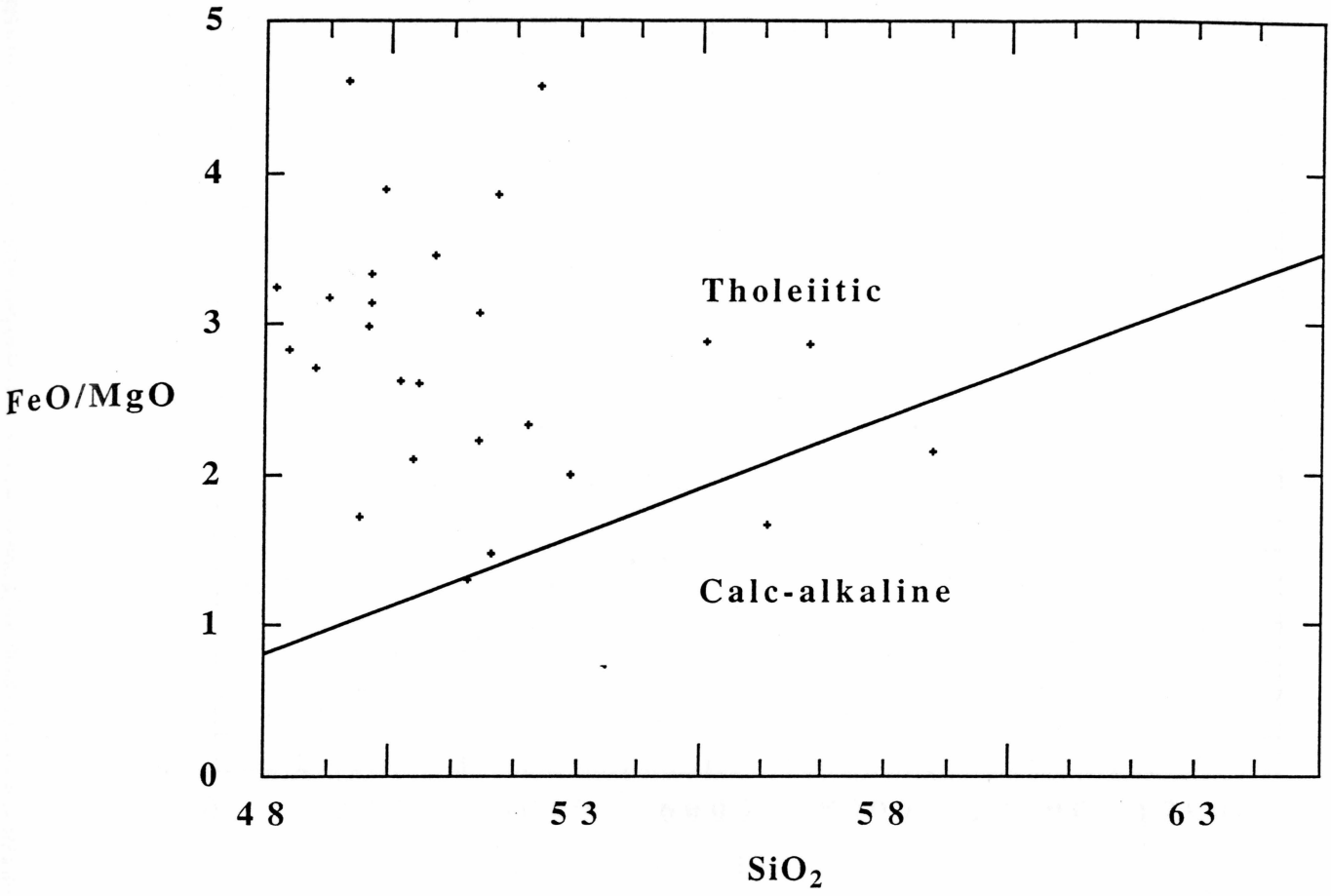

Figure 12: The SPMS amphibolites plot mostly as tholeiitic basalts on the FeO/MgO vs. SiO2 diagram (Miyashiro, 1974). Samples #12, #32, and #36B plot as calc-alkaline. The mobility of major elements may account for the discrepancy.

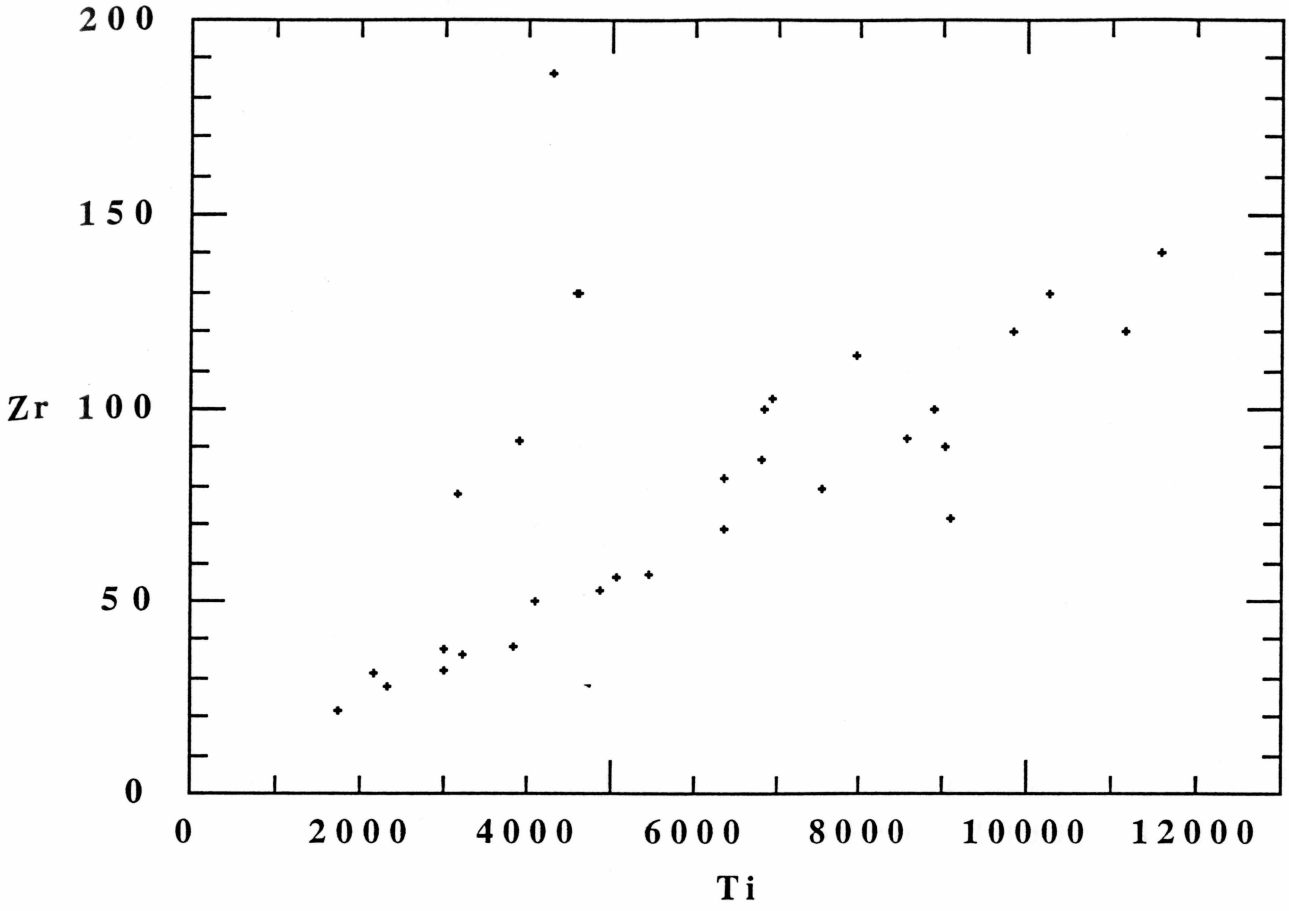

Figure 13: The SPMS amphibolites demonstrate positive slopes when plotted on a Zr vs. Ti diagram modeled after Cann (1970).

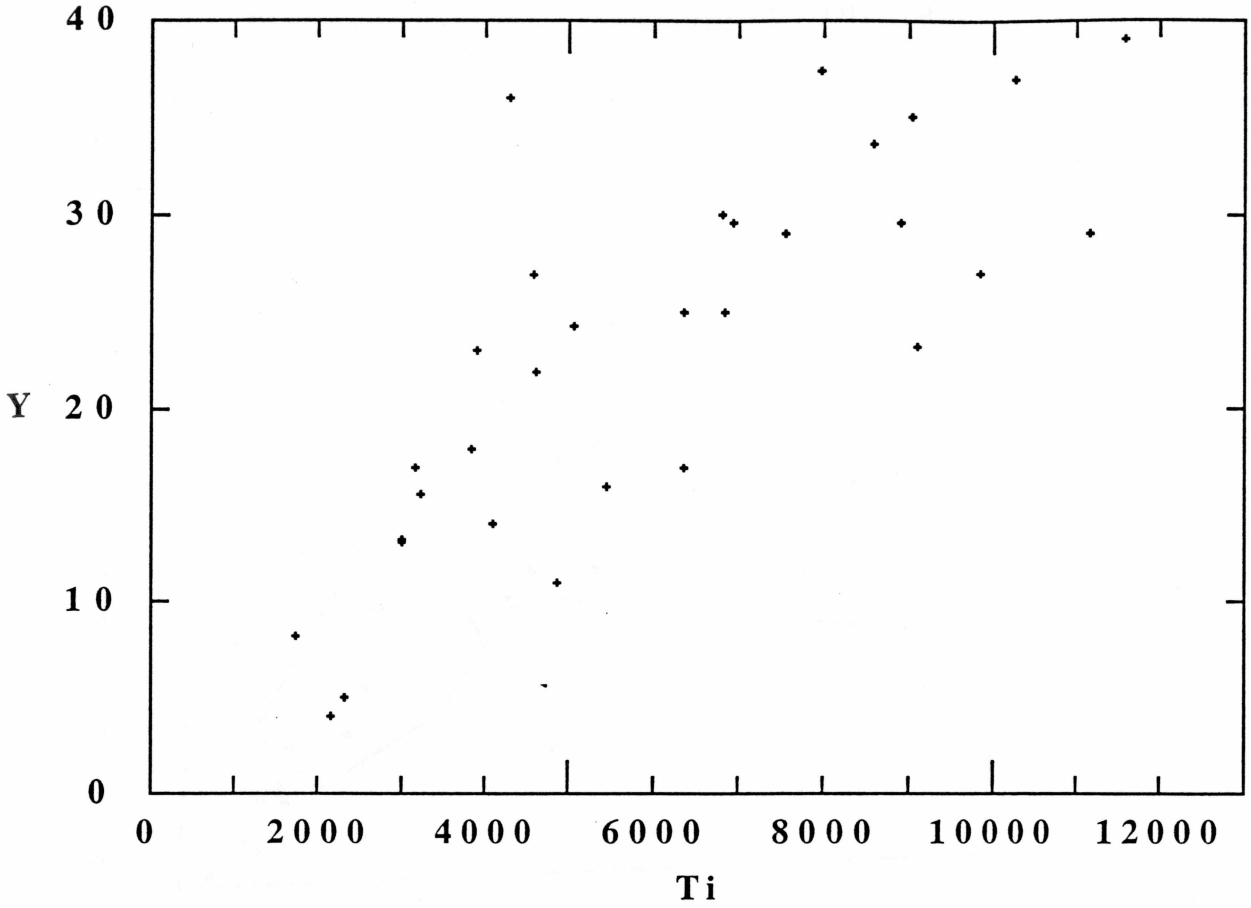

Figure 14: Y vs. Ti plot (Cann, 1970). The SPMS amphibolites show a positive slope indicative of an ocean-floor parent basalt.

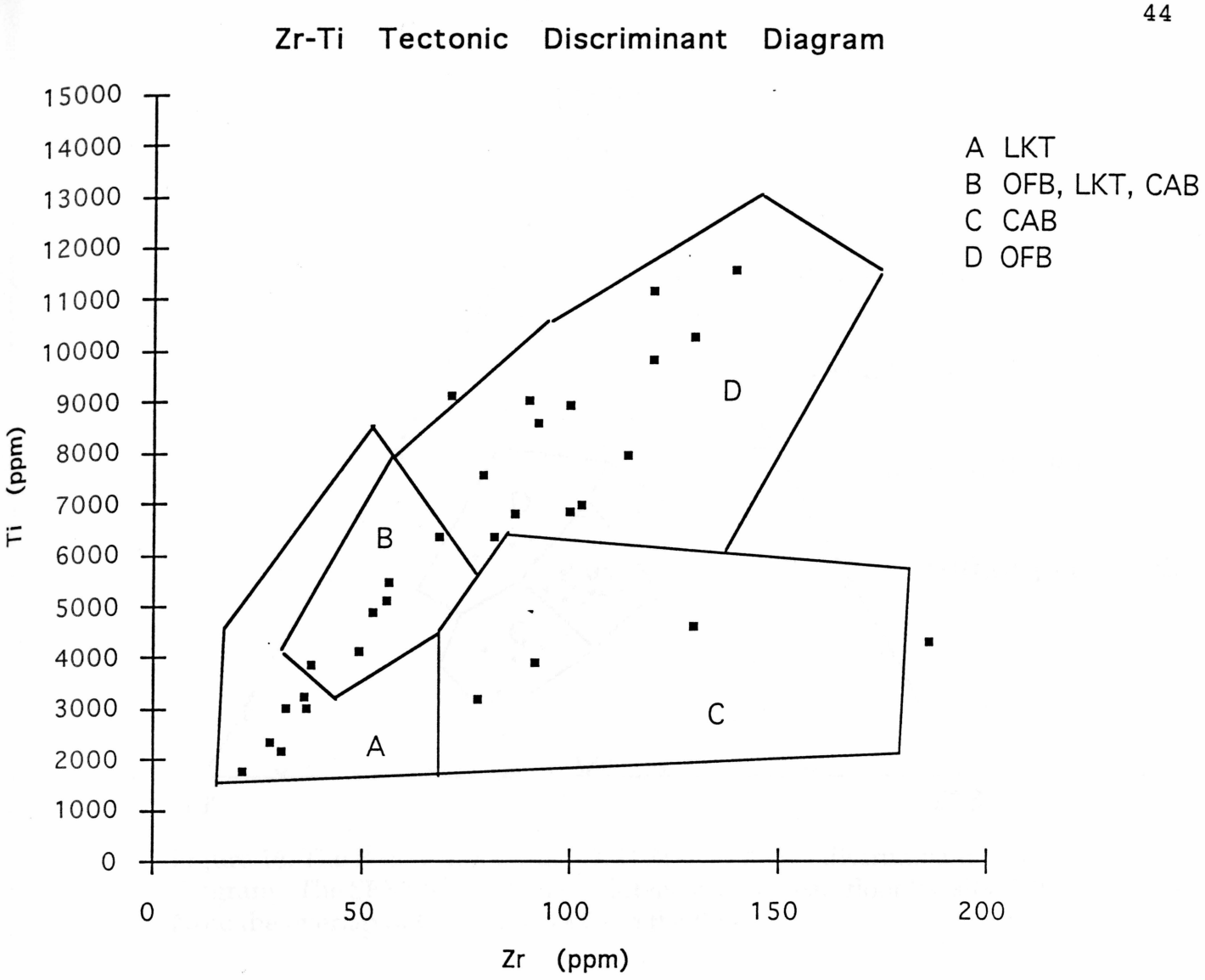

Figure 15: The SPMS amphibolites plot mostly as ocean-floor basalts (OFB) (14) and low potassium tholeiites (LKT) (6), associated with island-arc basalts, on the Ti-Zr discrimination diagram of Pearce and Cann (1973). 4 samples plot as calc-alkali basalts (CAB) and 6 plot in the field containing OFB, LKT, and CAB.

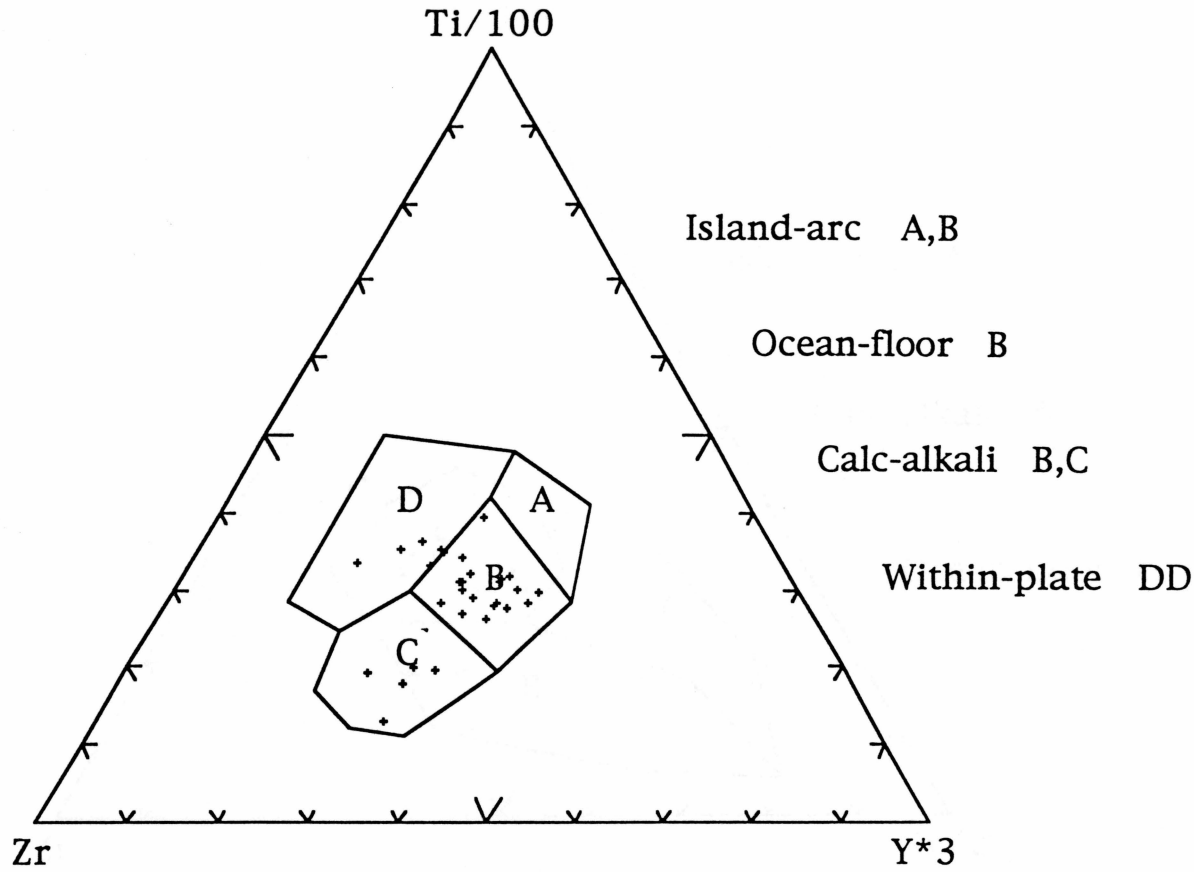

Figure 16: The Pearce and Cann (1973) Zr-Ti/100-Y*3 discriminant diagram. The SPMS amphibolites plot mostly as ocean-floor basalts (24). Note the overlap of OFB's and IAB's in the B field.

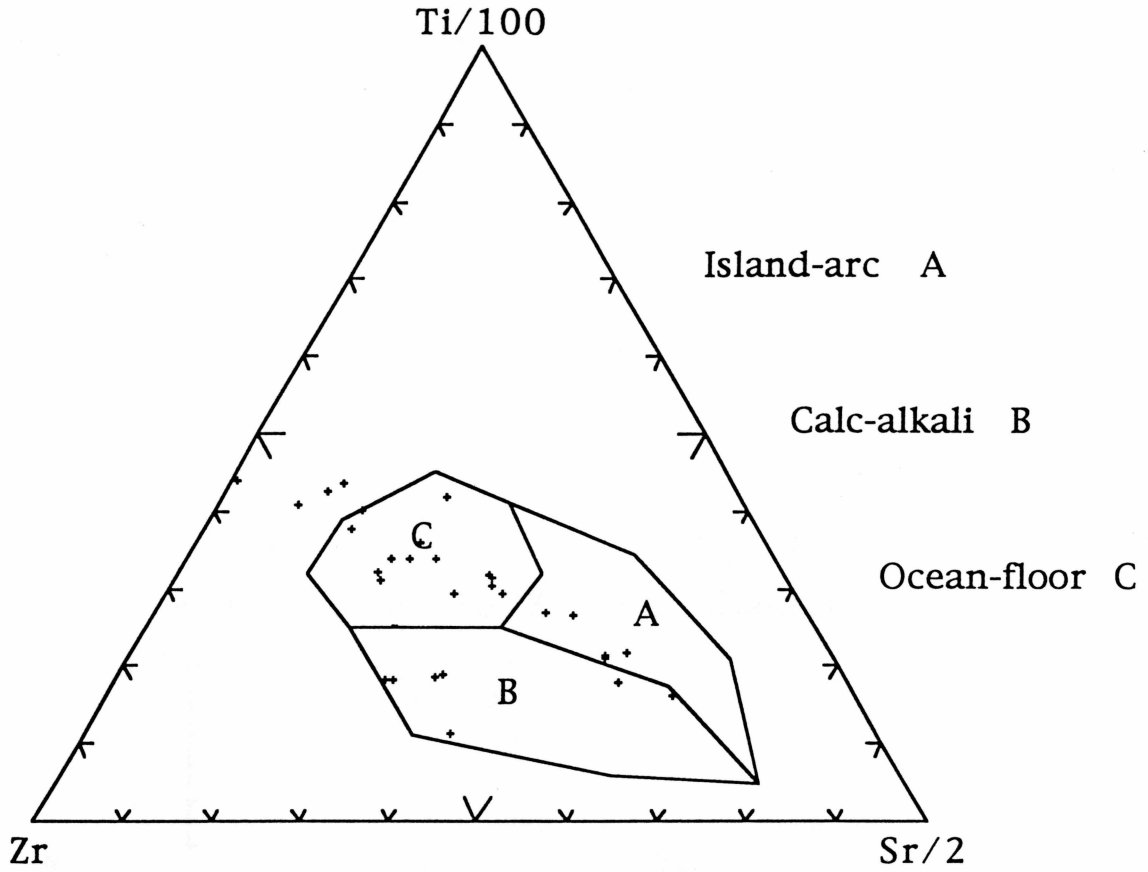

Figure 17: The Pearce and Cann (1973) diagram of Zr-Ti/100-Sr/2. Most of the SPMS amphibolites (13) plot in the field of ocean-floor basalts (OFB). 7 samples plot as calc-alkali basalts (CAB), 5 as island-arc basalts (IAB), and 4 outside the limits of OFB.

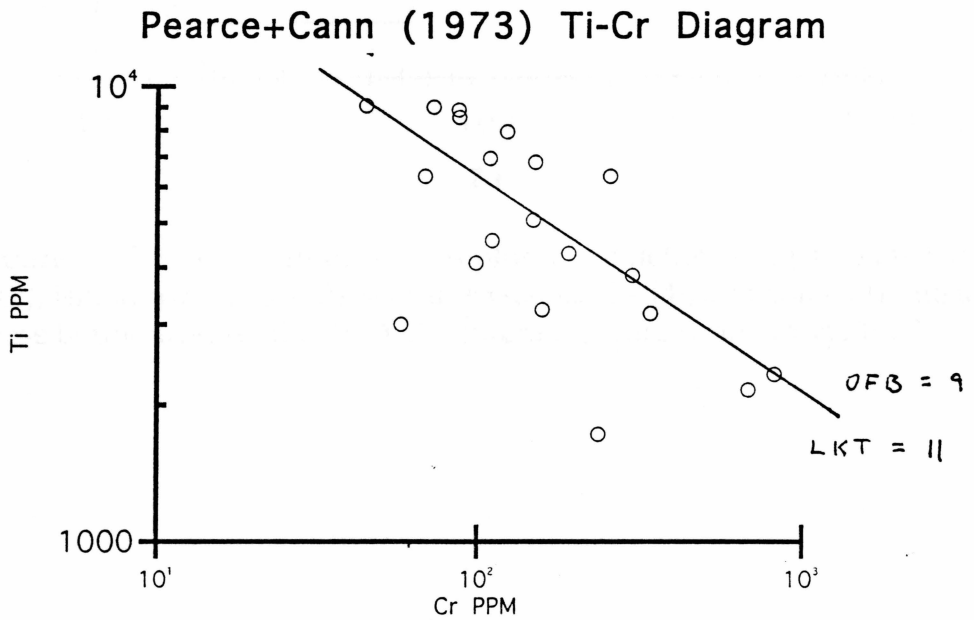

Figure 18: On the Ti vs. Cr discrimination diagram (Pearce and Cann, 1973), 20 of the 31 SPMS amphibolites plot as low-K tholeiites (11) and ocean-floor basalts (9).

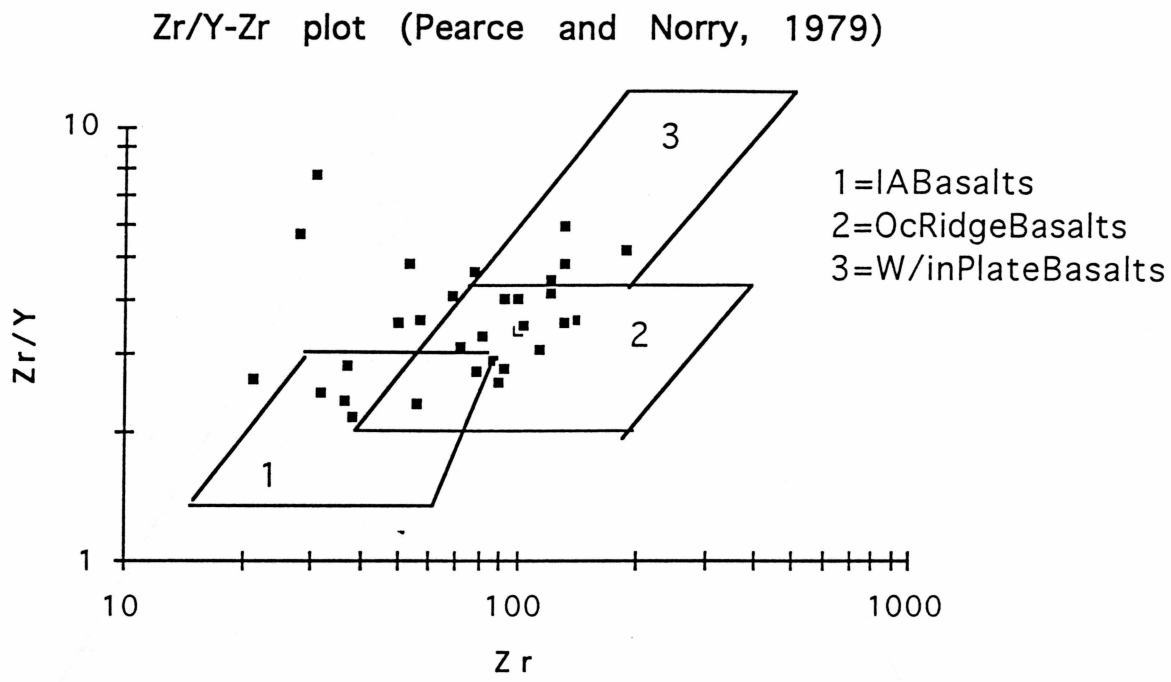

Figure 19: The SPMS amphibolites plot in the fields of ocean-ridge basalts (12), island-arc basalts (7), within-plate basalts (4), and some (8) outside these boundaries on the Zr/Y-Zr diagram (Pearce and Norry, 1979).

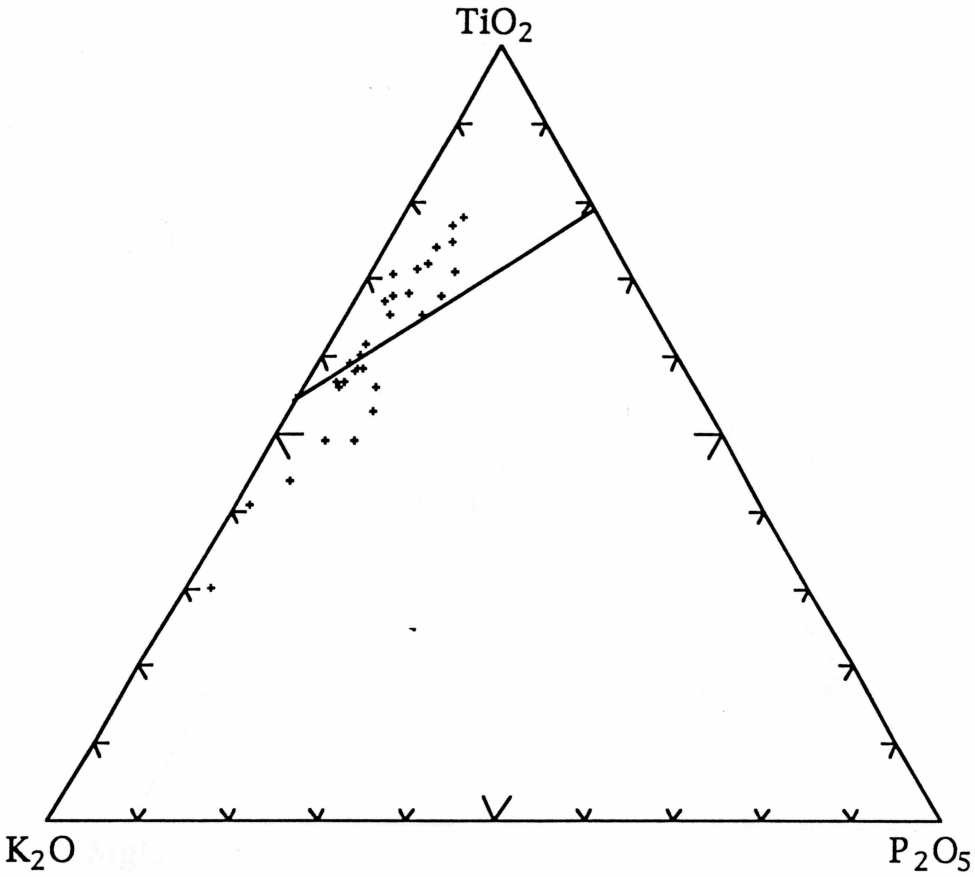

Figure 20: T.H. Pearce et al. (1975): Plot of SPMS amphibolites on a TiO2-K20-P2O5 plot, showing the dividing line between the oceanic field (upper portion) and the non-oceanic field (lower portion).

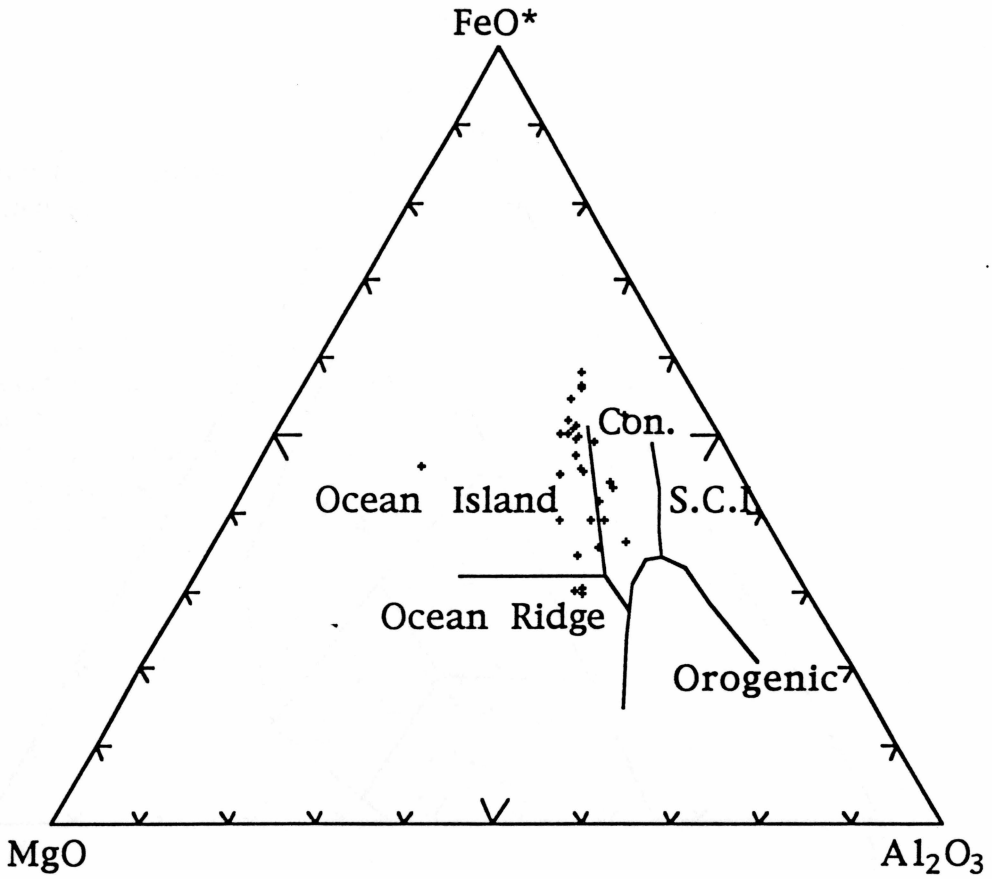

Figure 21: The Pearce et al. (1977) plot of MgO-FeO(total)-Al2O3. The SPMS amphibolites plot in the fields of ocean-island basalts (20), continental basalts (6), and ocean ridge/floor basalts (3). S.C.I.=Spreading Center Island Basalts.

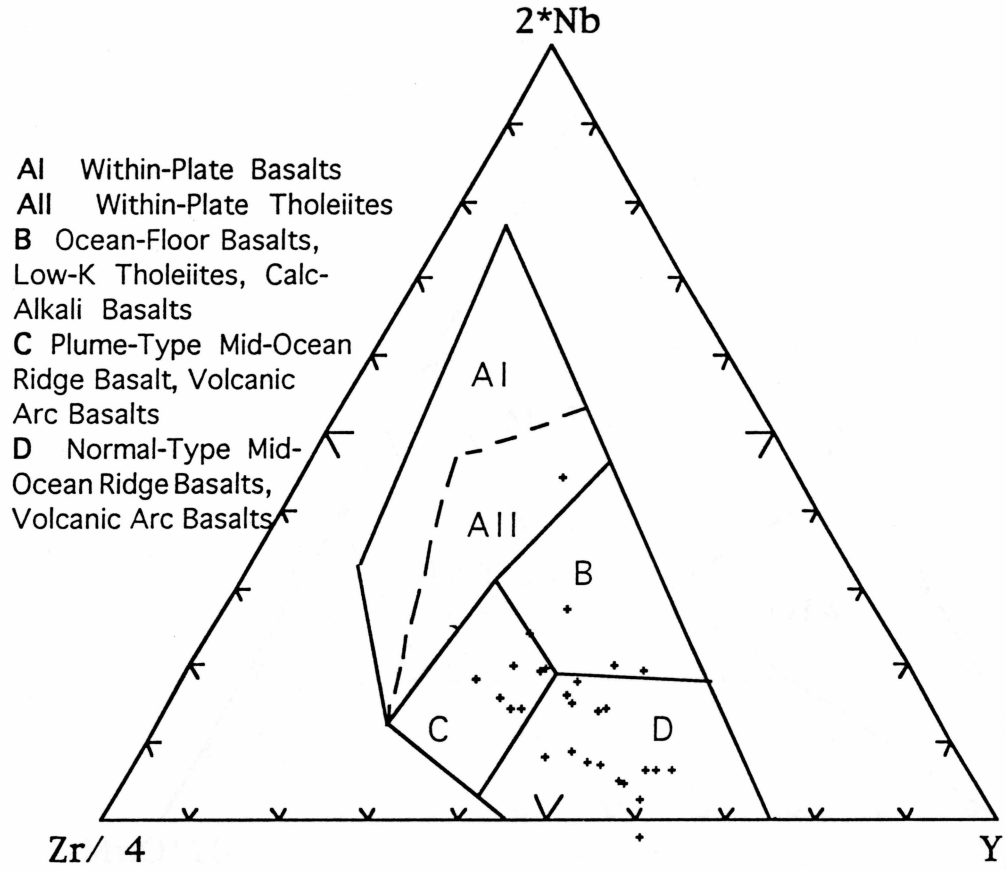

Figure 22: The SPMS amphibolites plotted on the Meschede (1986) Nb-Zr-Y diagram. Meschede does not reasonably differentiate the fields of MORB's and VAB's.

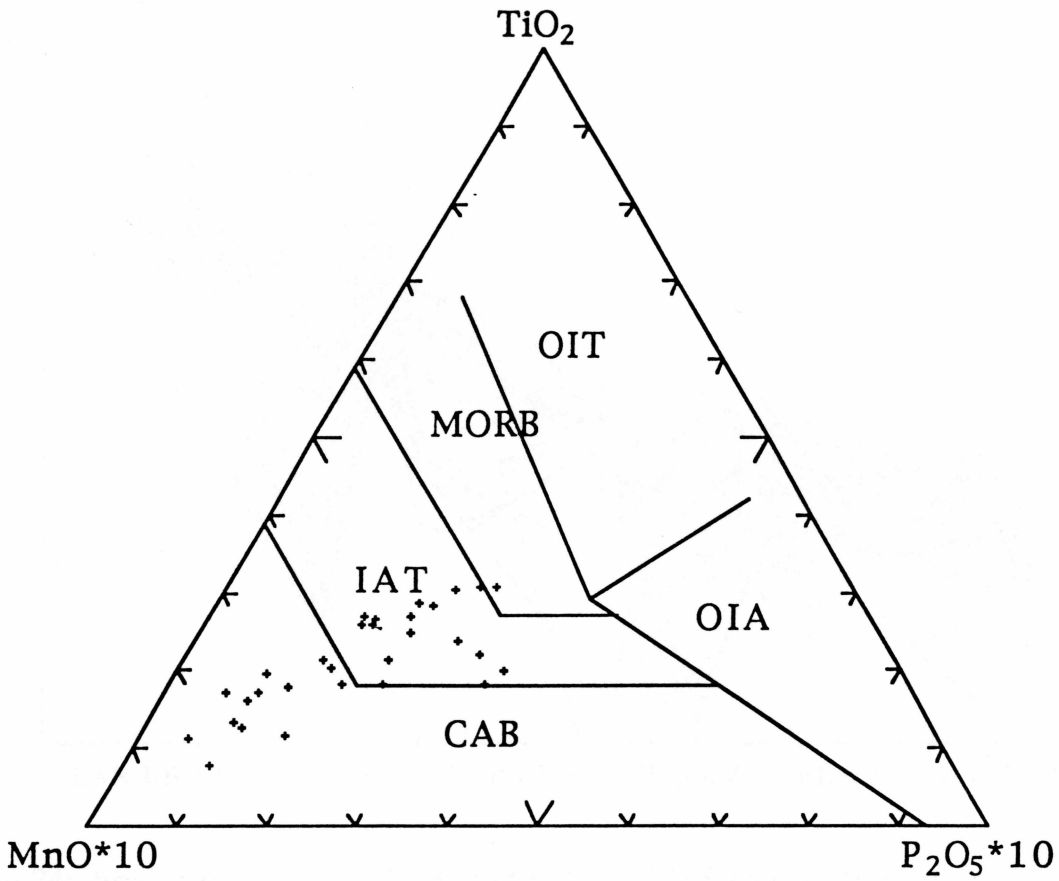

Figure 23: The Mullen (1983) MnO*TiO2-P2O5*10 diagram. OIT=Ocean-Island Tholeiites, MORB=Mid-Ocean Ridge Basalts, IAT=Island Arc Tholeiites, and CAB=Calc-Alkali Basalts. The SPMS amphibolites plot mainly as IAT (14) and CAB (13).

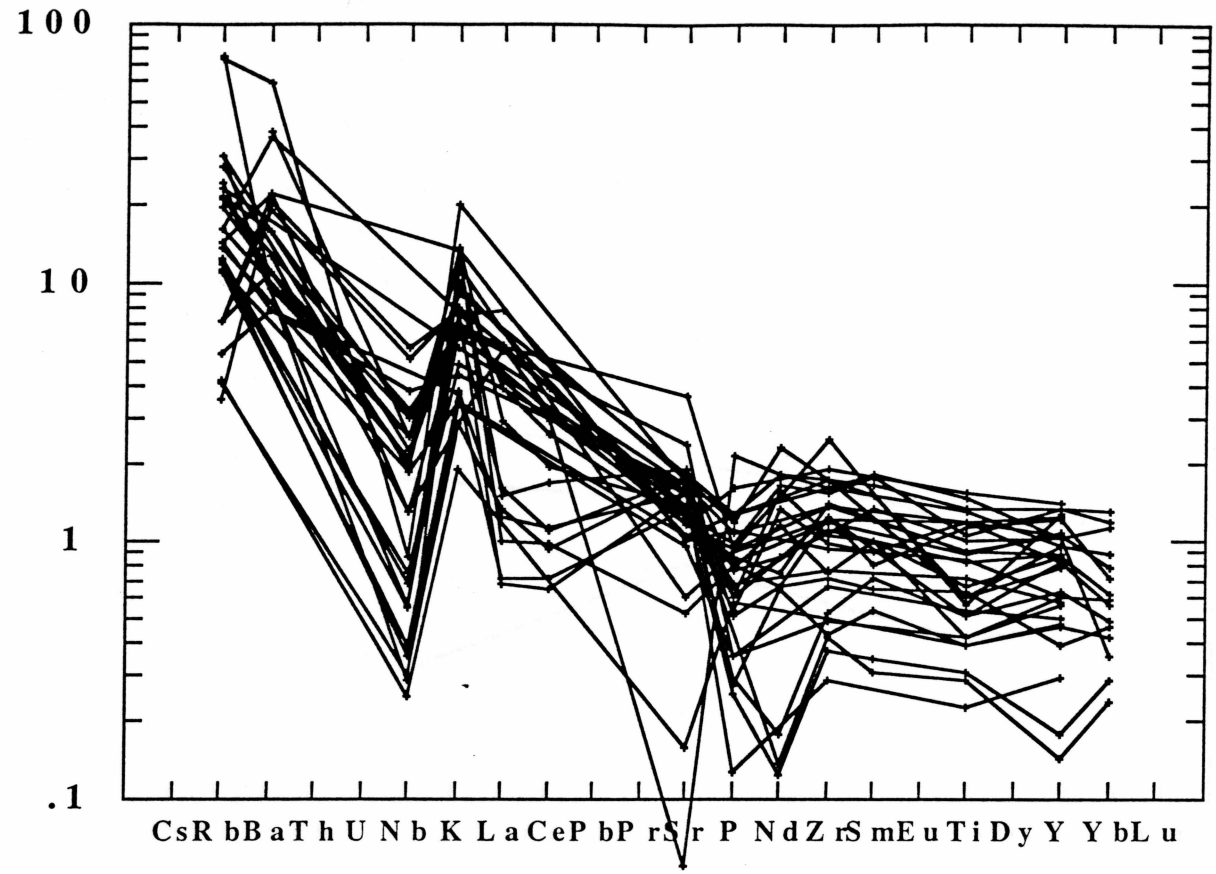

Figure 24: Spider diagram of the 31 individual SPMS amphibolite samples. Trace elements normalized to normal-type MORB (Sun and McDonough, 1989). Note the depletion in Nb, a characteristic signature of arc environments.

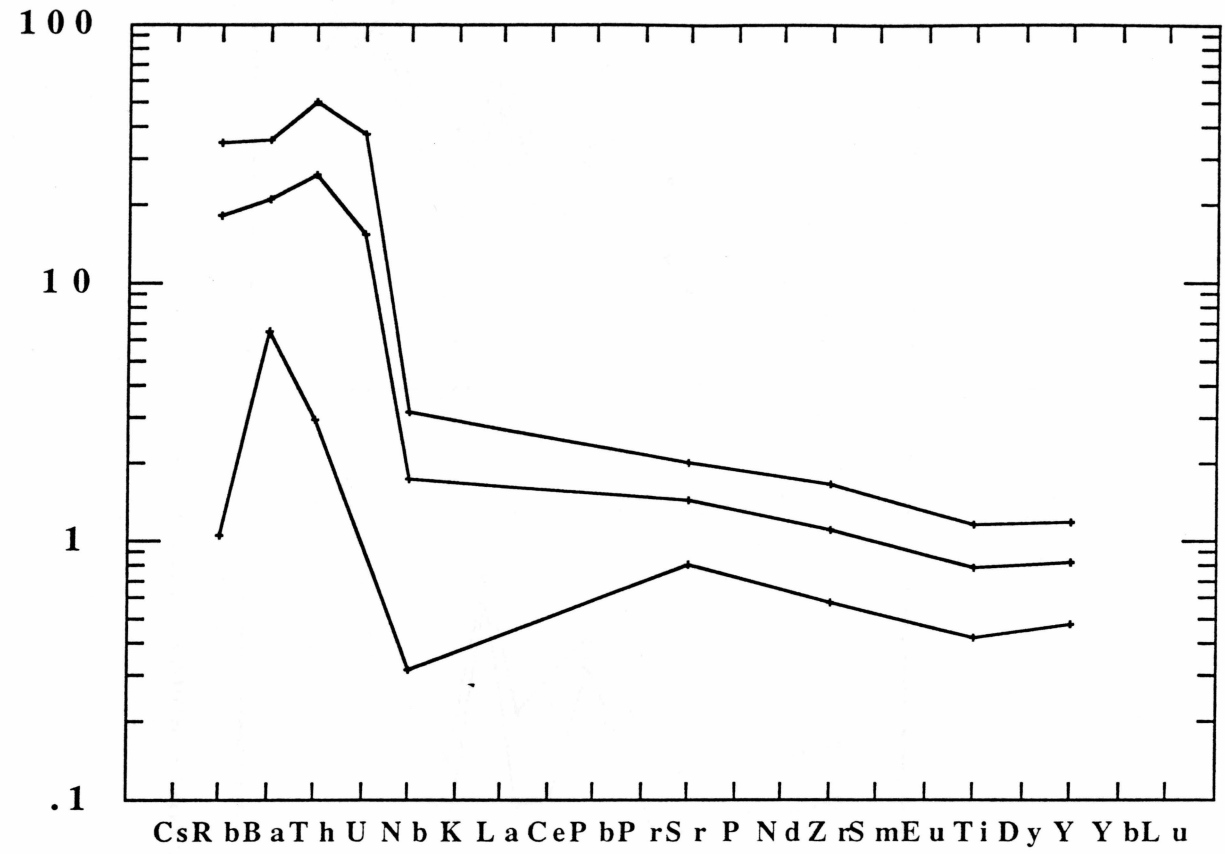

Figure 25: The nMORB normalized mean trace element values + or - one standard deviation for the 31 SPMS amphibolite samples.

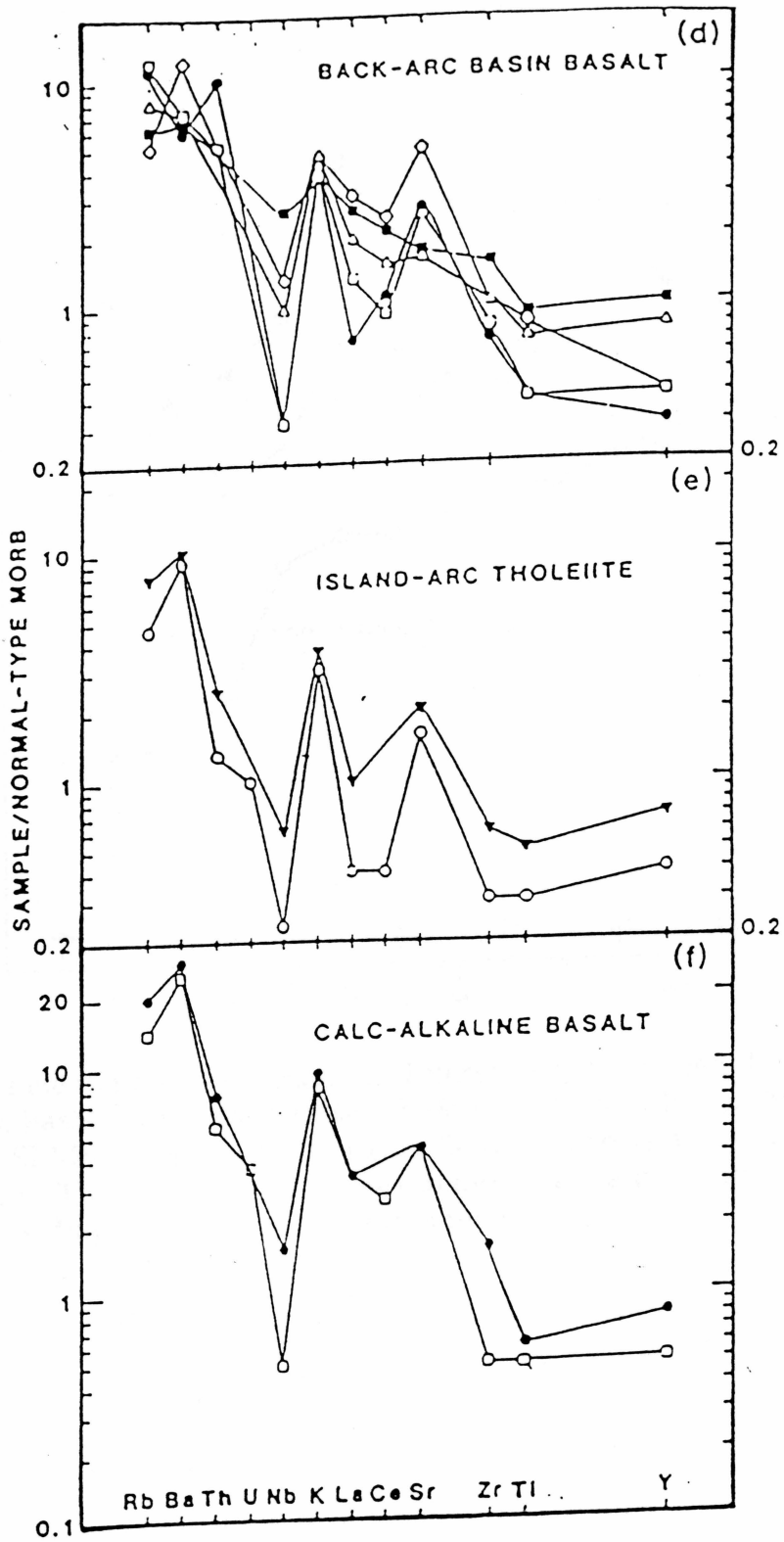

Figure 26: N-MORB-normalized patterns for various basalts (Weaver et al., 1979, and Saunders and Tarney, 1979). The SPMS amphibolites in figure 20 demonstrate a close connection to the pattern given by back-arc basin (BAB) basalts from the Bransfield Strait and Scotia Sea.

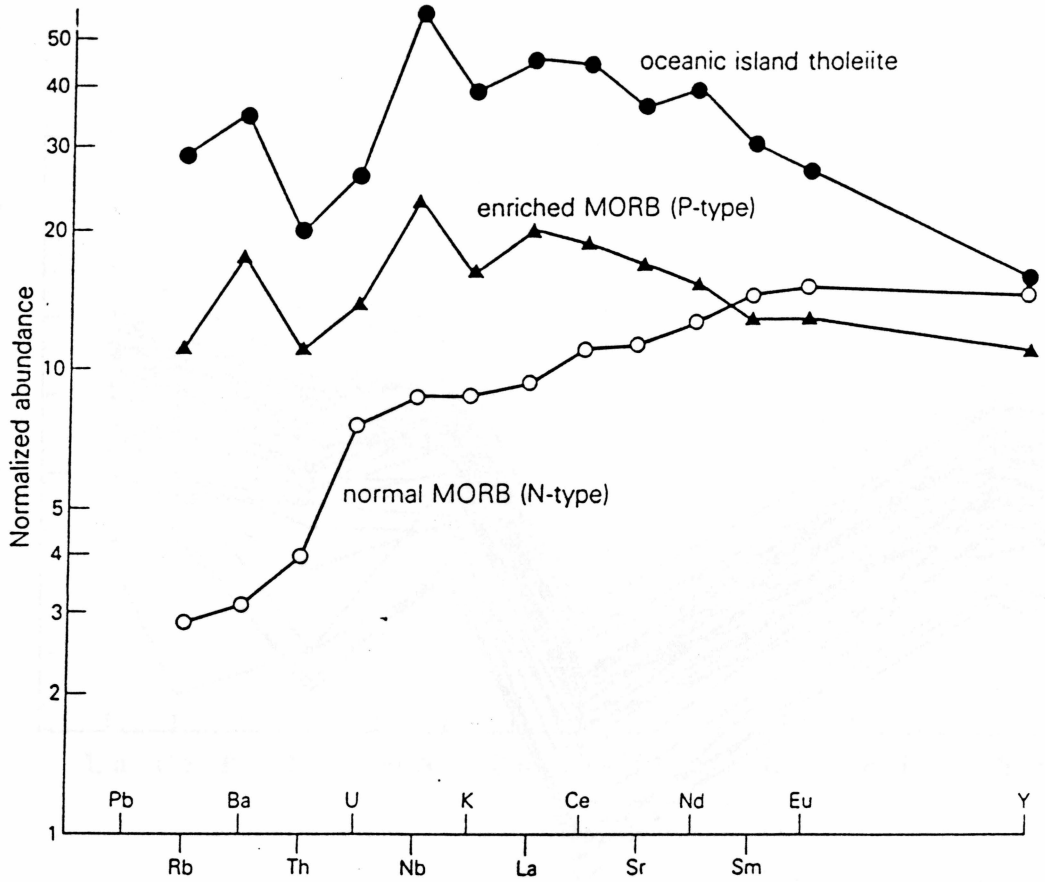

Figure 27: Trace element spider diagrams differentiating between different types of mid-ocean ridge basalts and ocean island tholeiites (Wilson, 1989). Note that the patterns for the SPMS amphibolites in figure 20 do not correlate very well with the ones shown here. The SPMS amphibolites demonstrate a depletion in Nb, while the basalts in this diagram show a Nb enrichment.

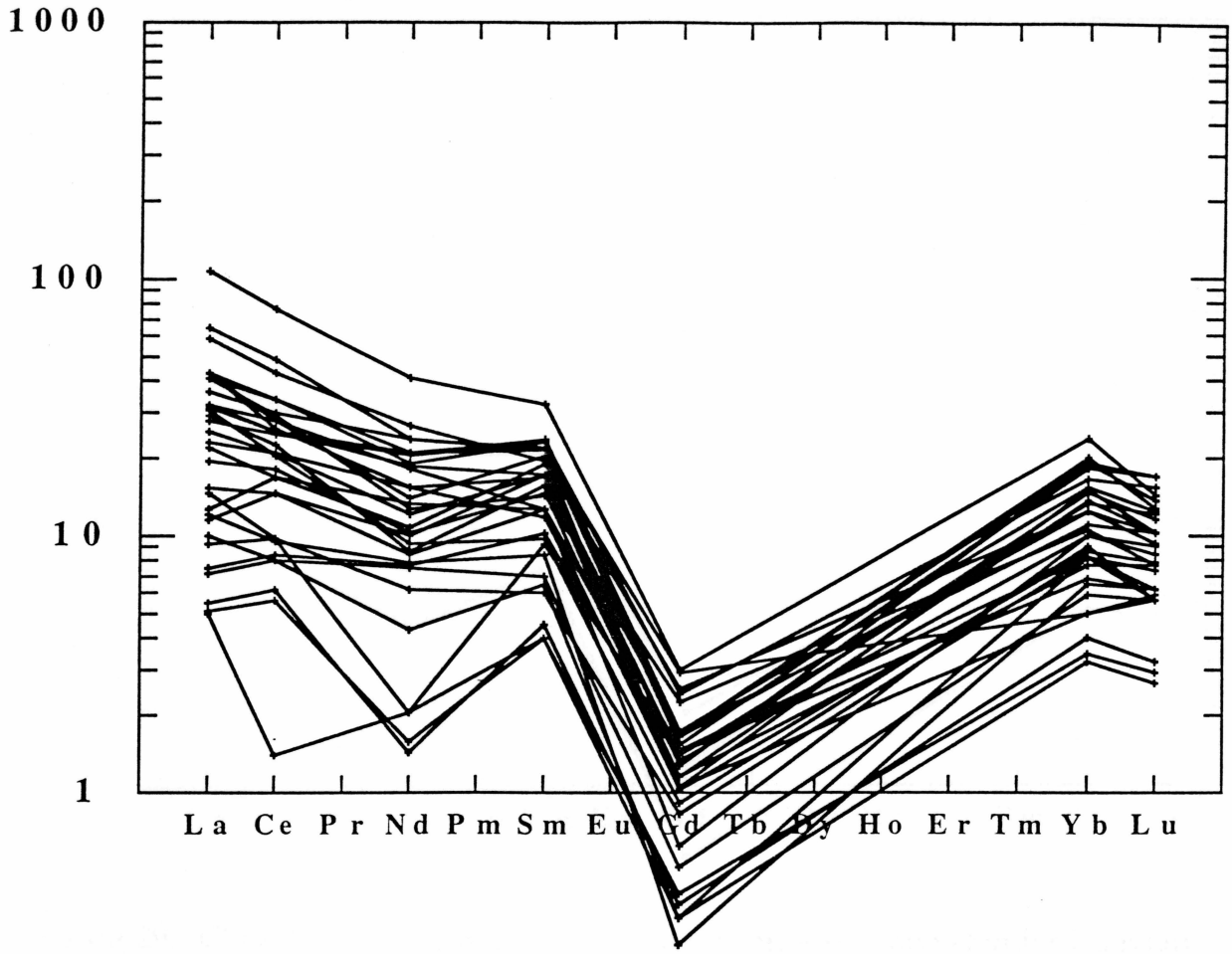

Figure 28: Chondrite-normalized plot of REE for the 31 SPMS amphibolite samples. Several of the samples (#6, #21B, #29D, #32, #33D, and #39C) demonstrate notable depletions in Nd. Sample #33D also shows an unusual depletion in Ce. All samples have an anomalous and extreme depletion in Gd.

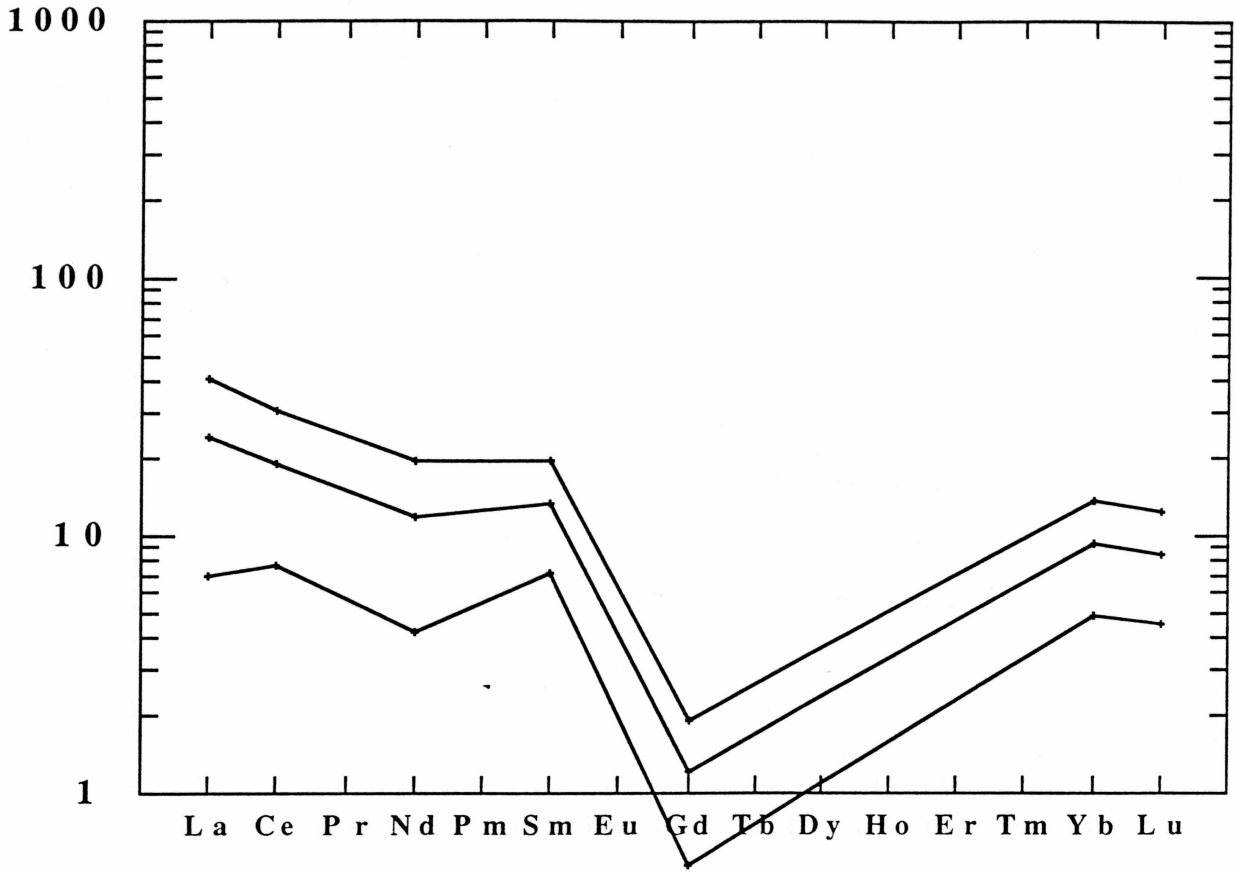

Figure 29: Chondrite-normalized plot of the mean + or - one standard deviation for the REE concentrations in the 31 samples of SPMS amphibolites.

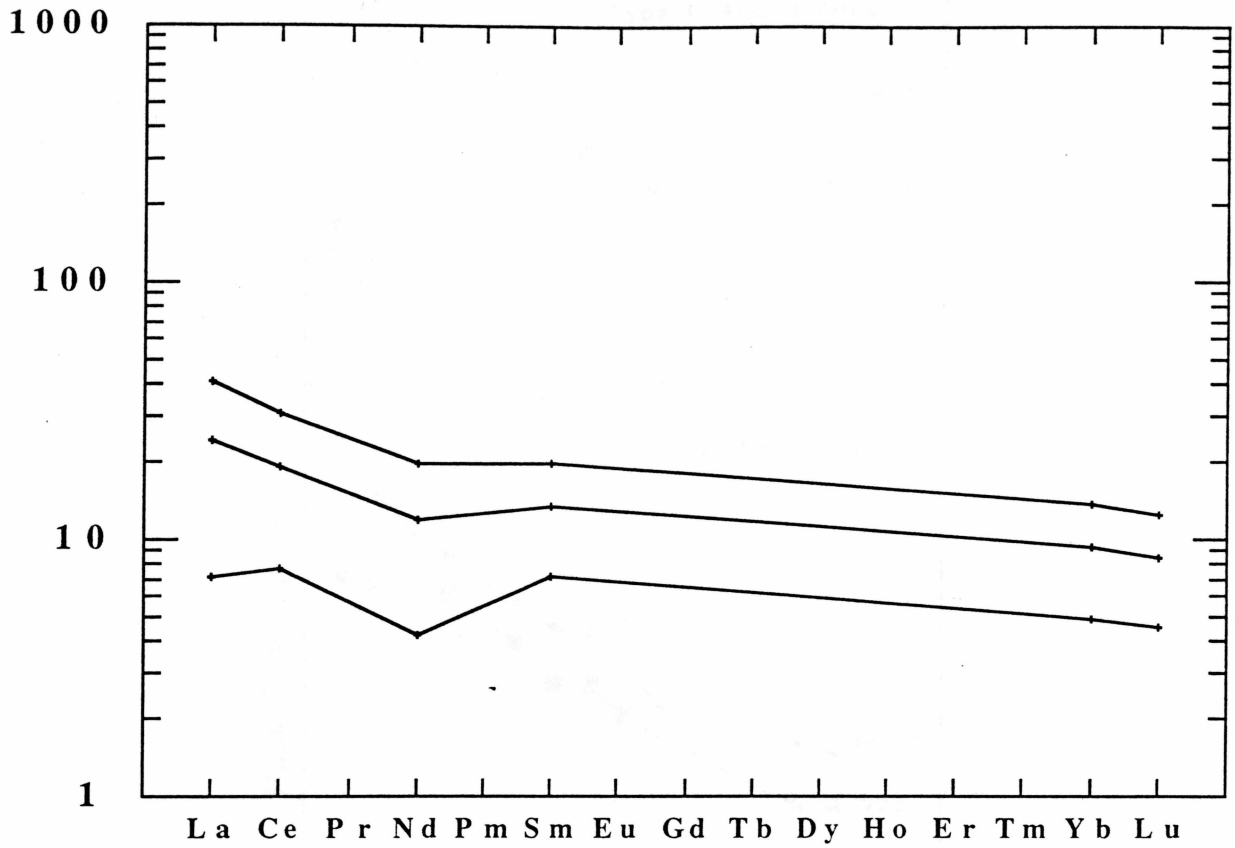

Figure 30: REE plot for the SPMS amphibolites with the depleted Gd concentrations removed.

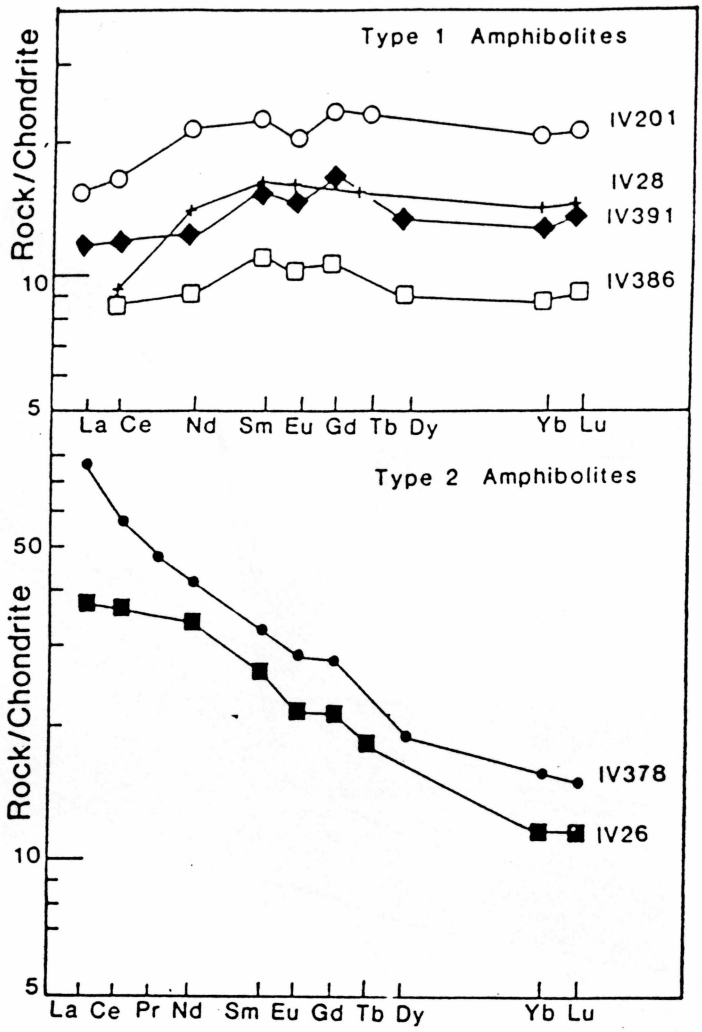

Figure 31: Two different REE patterns for amphibolites from the Ivrea Zone, Southern Alps, Northwest Italy (Sills and Tarney, 1984). These amphibolites demonstrate a slight enrichment in Gd, while the SPMS amphibolites show an anomalous depletion in Gd.

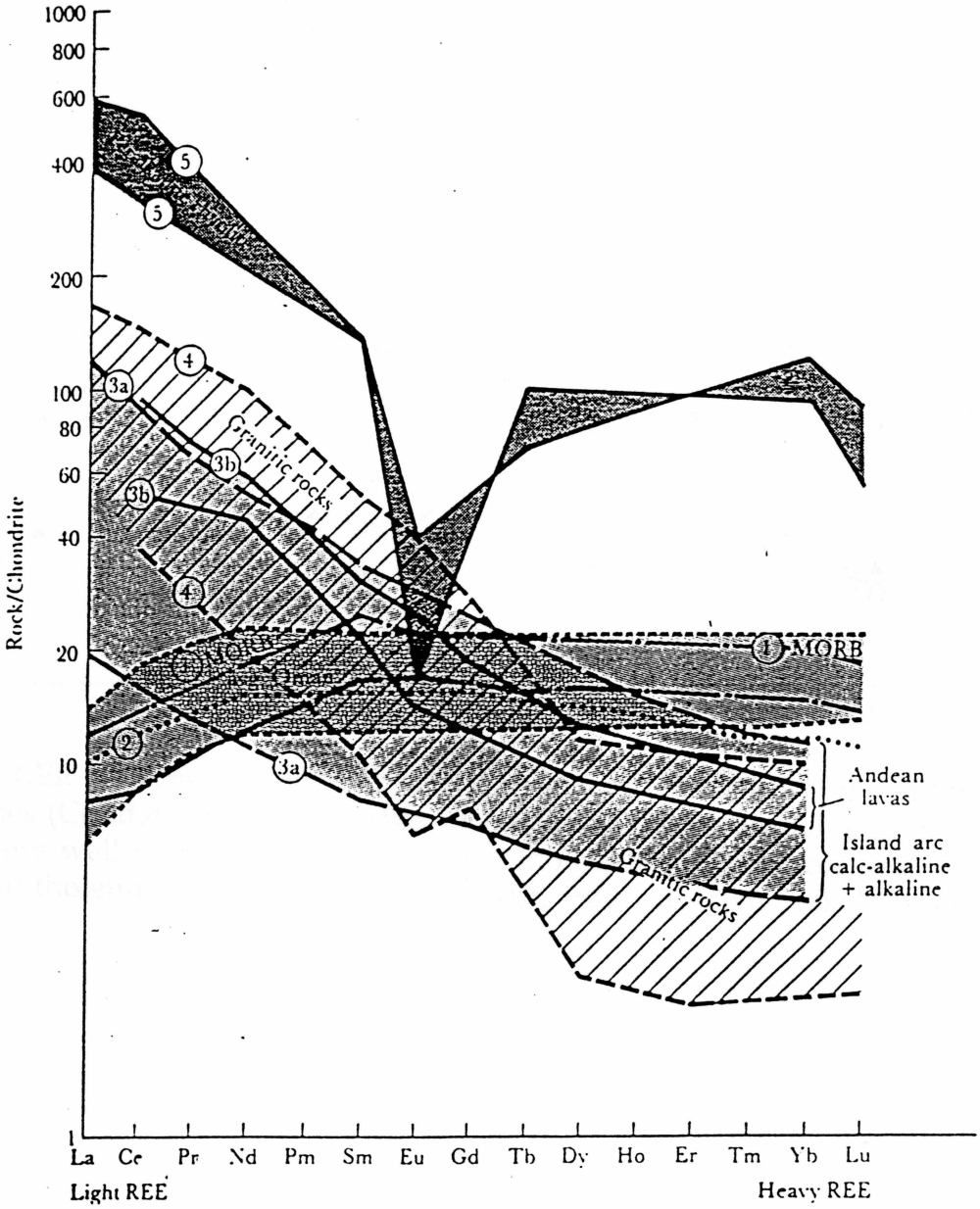

Figure 32: Chondrite-normalized REE patterns for various basalt-types (Hyndman, 1985). Notice how the REE patterns for the SPMS amphibolites in figure 23 do not correlate with just one pattern but seem to fall in the fields for many types of basalts and granite. 1=MORB, 2=Oman ophiolite, 3a=island arc volcanic rocks, 3b=Andean lavas, 4=granitoid rocks, granite to tonalite, 5=peralkaline rhyolite.

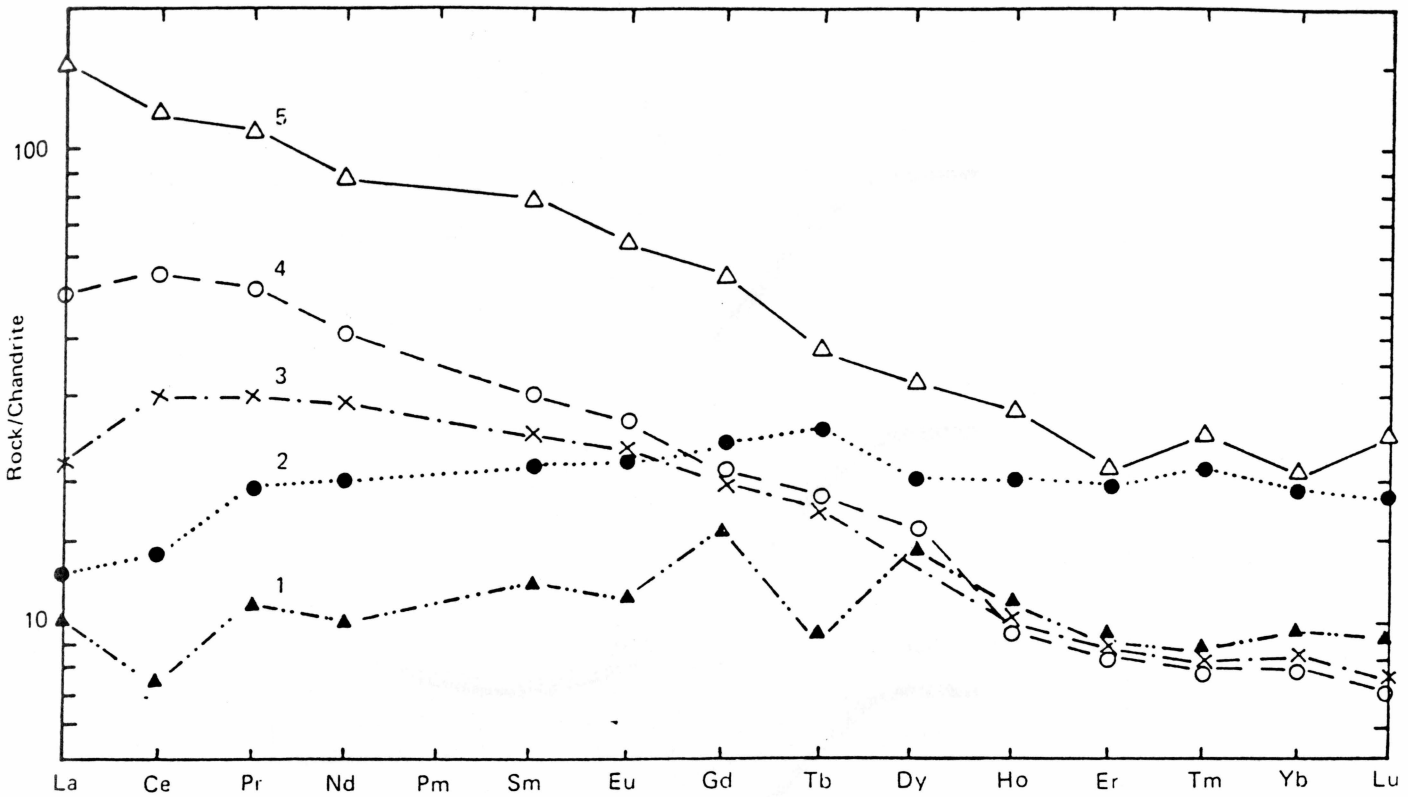

Figure 33: REE patterns for various types of basalts as compared to the SPMS amphibolites (Condie, 1976). REE patterns for the SPMS amphibolite do not seem to correlate very well with these basalts. 1=Arc tholeiites, 2=Rise tholeiites, 3=Hawaiian tholeiites, 4=Hawaiian alkali basalt, 5=Ocean-island alkali basalt.

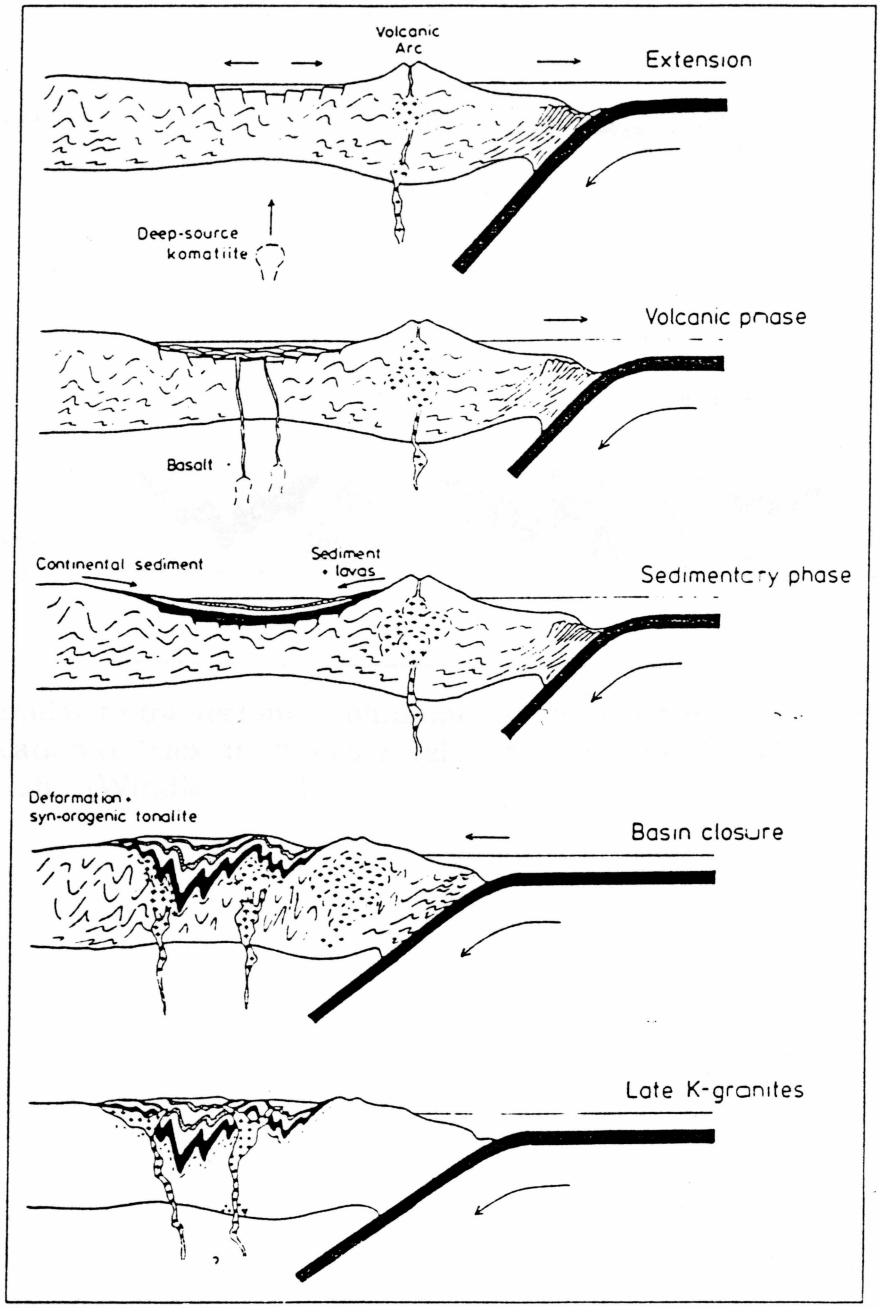

Figure 34: Diagram demonstrating a possible scenario for the development of a back-arc basin during the Archean (Windley, 1984).

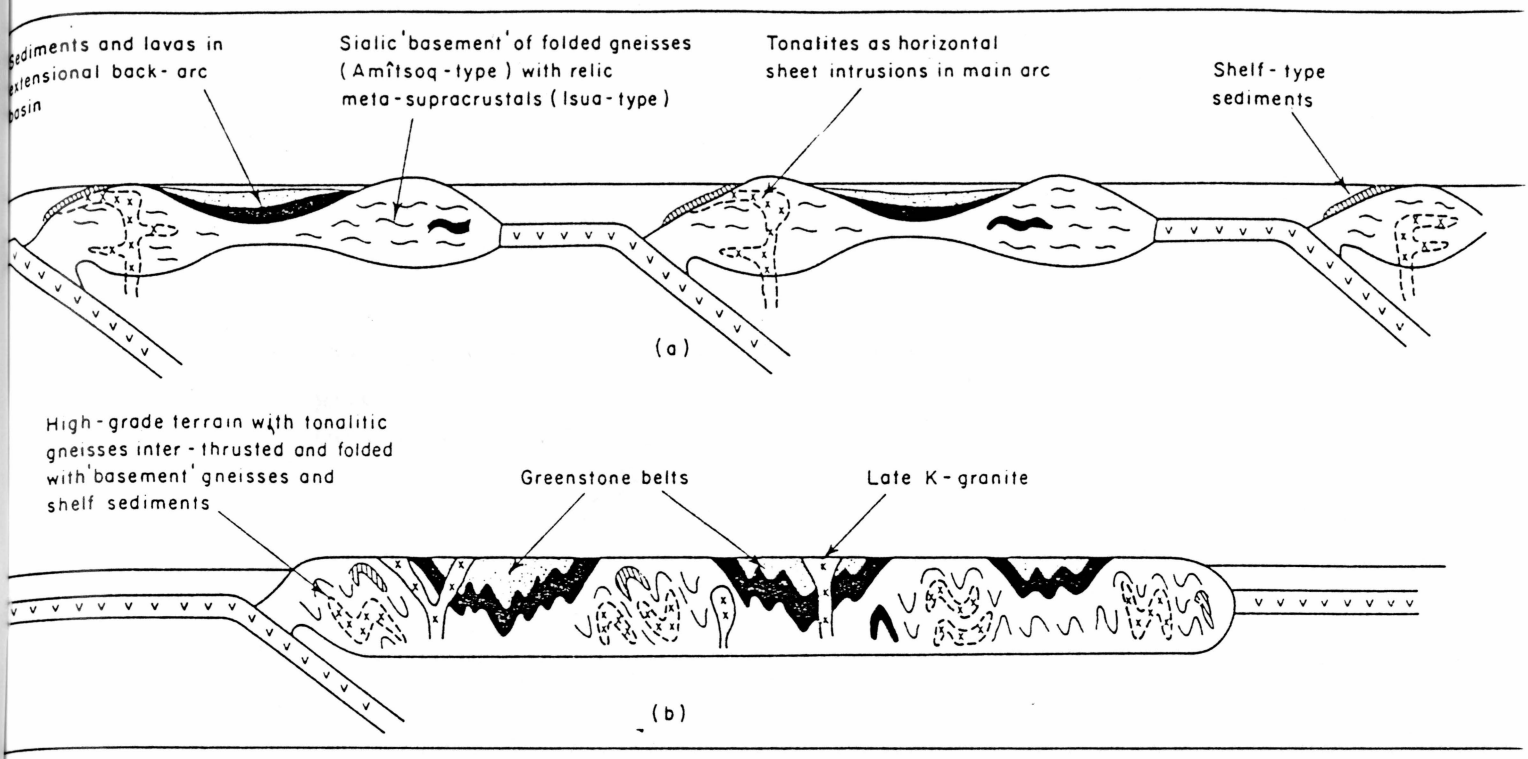

Figure 35: Similar to the tectonic environments presented in table 12, this diagram shows the location of back-arc basins in relation to proposed Archean mini-continental plates (Windley, 1984).

On my honor I pledge that I have neither given nor received any unacknowledged aid on this assignment.